AD-761 654

DEVELOPMENT OF CAPABILITIES OF OPTICAL DIFFRACTION ANALYSIS FOR QUANTITATIVELY COMPARING AND CORRELATING ROCK FABRICS AND FABRIC CHANGES

WISCONSIN UNIVERSITY

PREPARED FOR
ADVANCED RESEARCH PROJECTS AGENCY

JUNE 1973

DEVELOPMENT OF CAPABILITIES OF OPTICAL DIFFRACTION ANALYSIS FOR QUANTITATIVELY COMPARING AND CORRELATING ROCK FABRICS AND FABRIC CHANGES

Second and Final Technical Report (Jan. 14, 1972 - May 2, 1973) Report due June 14, 1973

ARPA ORDER NO. 1579 Amend. No. 3
Program Code No. 2F10

CONTRACTOR - UNIVERSITY OF WISCONSIN
(U.W. Acct. No. 144-C628)

Effective date of contract:
January 14, 1972

Contract Expiration date:
Initially January 13, 1973,
extended three months to
April 13, 1973

Amount of contract:
$43,816

Monitored by U.S. Bureau of Mines
Contract No. HO220016

Principal Investigator:
Professor H. J. Pincus
Department of Geological Sciences
University of Wisconsin-Milwaukee
Milwaukee, Wisconsin 53201
Tel. (414) 963-4017
-4561

Project Engineer:
Mr. Robert C. Steckley
Twin Cities Mining Research Center
P.O. Box 1660
Twin Cities, Minnesota 55111
Tel. (612) 725-4583, 4570

Sponsored by:
Advanced Research Projects Agency
ARPA Order No. 1579, Amend. No. 3
Program Code No. 2F10

Note: This annual technical report is submitted in compliance with Sec. 2.8, p. 9 of the contract and Data and Reporting Clause, para. (b) (1), pp. 14, 15 of Appendix A, General Provisions.

Prepared by:

Howard J. Pincus June 14, 1973
Professor Howard J. Pincus
Principal Investigator

DOCUMENT CONTROL DATA - R & D

(Security classification of title, body of abstract and indexing annotation must be entered when the overall report is classified)

1. ORIGINATING ACTIVITY (Corporate author)

University of Wisconsin

2a. REPORT SECURITY CLASSIFICATION

Unclassified

2b. GROUP

3. REPORT TITLE

Development of Capabilities of Optical Diffraction Analysis for Quantitatively Comparing and Correlating Rock Fabrics and Fabric Changes.

4. DESCRIPTIVE NOTES (Type of report and, inclusive dates)

Second and Final Technical Report, Jan. 14, 1972-May 2, 1973

5. AUTHOR(S) (First name, middle initial, last name)

Professor Howard J. Pincus
Department of Geological Sciences
University of Wisconsin-Milwaukee

6. REPORT DATE	7a. TOTAL NO. OF PAGES	7b. NO. OF REFS
June 14, 1973		87

8a. CONTRACT OR GRANT NO.	9a. ORIGINATOR'S REPORT NUMBER(S)
HO220016	Second and Final Tech. Rept. (Acct. 144-C628)
b. PROJECT NO ARPA Order No. 1579 Amend. 3, Program Code No. 2 F10 (62701D)	
c.	9b. OTHER REPORT NO(S) (Any other numbers that may be assigned this report)
d.	

10. DISTRIBUTION STATEMENT

Distribution of the document is unlimited

11. SUPPLEMENTARY NOTES	12. SPONSORING MILITARY ACTIVITY
	Director Advanced Research Projects Agency Washington, D. C. 20301 Att: Program Mgmt.

13. ABSTRACT

Standard uniaxial loading of rock specimens and cantilever and third-part loading of rock slices cemented to aluminum beams have provided input data. Fabrics of rock specimens undergoing deformation have been recorded photographically in white light, in ultra-violet illumination after treatment of specimens with fluorescent dye penetrants, and with acetate peels. These fabric pictures have been converted to their two-dimensional Fourier amplitude transforms by optical diffraction. Changes in the transforms reflect spatial changes in the fabrics with loading.

Transforms have been produced from petrographic thin sections using a modified laboratory microscope and partially coherent light; this technique promises wider application of optical diffraction analysis in petrofabric studies. An extensive collection of reference inputs and their transforms has been prepared.

Experimental results show the capability of detecting changes in width, orientation, and frequency of lineaments related to loading. Differences in transforms may be used to characterize deformation and anisotropy.

ib

14 KEY WORDS	LINK A		LINK B		LINK C	
	ROLE	WT	ROLE	WT	ROLE	WT
Optical Diffraction Analysis	6	3				
Rock Fabric	7	3				
Rock Deformation	8	3			8	3
Reference Inputs and Fourier Transforms			5	1		
Maps of Fourier Transforms			5	1		
Fourier transforms Obtained with Laboratory Microscope			10	2		
Holographic Subtraction			10	0		

Table of Contents

List of Illustrations

(Figures accompanying text appear sequentially in Appendix A)

List of Tables

Technical Report Summary

The purposes of this project, as originally conceived for a three-year period, have been a) to develop capabilities of optical diffraction analysis for comparing and correlating suites of genetically related rock fabrics, and b) to contribute to the understanding of the mechancis of rock deformation by quantifying fabric changes and relating these to other deformation parameters.

Increased understanding of the relationships between fabric and mechanical behavior should lead to more accurate prediction of rock behavior in engineering operations, and ultimately to more effective design of structures in rock and of safer and more efficient excavation techniques.

This report is concerned primarily with the second year of research funded by ARPA, ending January 1973. A no-cost, three-month extension of the contract has provided additional opportunity for research.

Our general methodology has utilized two types of operation and their outputs, namely, experimental rock deformation and optical diffraction analysis.

Fabrics of rock specimens undergoing experimental deformation have been recorded on photographic film and acetate peels. These data have been used as inputs to the optical diffraction system. Optical outputs have consisted of transforms, profiles and maps of transforms and filtered reconstructed images.

Results indicate that the several fabric-based indexes that have been developed in this study for characterizing deformation and anisotropy are easily applied and generally useful. We have obtained results showing at least some positive connection between initial fabric and subsequent deformation fabric, non-directional properties such as grain-size and deformation fabric, extent of changes in fabric with increasing load and its approach to failure, and so forth. We have also shown that a microscope can be used to generate transforms directly from rock slices.

Increases and decreases in spatial frequency and directional changes in fabric elements can all be related in logical ways to deformation modes.

Our biggest operational bottleneck earlier in the project was in specimen production. This problem has now been surmounted. A significant changeover in supporting personnel in January caused some loss of output, but not of major proportions. Major technical problems have all been largely solved, bypassed, or mitigated.

Regarding DoD implications, the techniques and results developed here are indeed applicable to rapid excavation objectives and, in addition, much of the techniques developed are relevant to other research fields bearing on the national interest and dependent on spatial analysis of two-dimensional displays such as maps, slides, plotted curves, and so forth.

Further research to be undertaken will involve further analysis of data already on hand, study of additional rock types, comparison of experimentally deformed rocks with rocks that have failed under field conditions, study of triaxially deformed rocks, and optical diffraction analysis in reflected light to render field application more feasible.

Introduction - Purpose and Objectives

The purposes of this project, as originally conceived for a three-year time span, have been:

(a) to develop capabilities of optical diffraction analysis for comparing suites of genetically related rock fabrics, and
(b) to contribute to the understanding of the mechanics of rock deformation by quantifying fabric changes and relating these to other deformation parameters.

The component objectives of the study are as follows:

(a) To develop quantitative methods using optical diffraction in order to compare and correlate fabrics of a deformation series so that changes in fabric can be related to deformation curves and other quantitative deformation data.

(b) To identify and characterize through spatial frequency analysis the critical fracture parameters associated with failure.

(c) To develop a system of standarized fabric patterns and reference transforms with which fabric inputs can be correlated quantitatively.

(d) To develop an index of deformation in terms of fabric change, from one input to the next, and to relate this index to deformation history.

(e) To develop an index of fabric heterogeneity for different directions in a single specimen, to be compared with anisotropy measures based on directional differences in physical behavior in the same specimen.

(f) To compare fabrics in experimentally deformed rocks with those in several selected equivalent rocks that failed under field conditions.

Increased understanding of the relationships between fabric and mechanical behavior should lead to more accurate prediction of rock behavior in engineering operations, and ultimately to more effective design of structures in rock and of safer and more efficient excavation techniques.

This report is concerned primarily with the second year of research funded by ARPA, ending January 1973. A no-cost, three month extension of the contract has provided additional opportunity for research. With a grant of $6000 from the Graduate School of the University of Wisconsin-Milwaukee, it has been possible to stage a full-semester's operation at a reduced level of activity

beyond the January 1973 termination date. Some of the results of this University-supported work are reported herein; additional results will be forthcoming in published articles.

With the termination of ARPA support resulting from the roll-back in funding of ARPA's Rapid Excavation Program, it has obviously not been feasible to complete in 24 months (or 27 months, with the three-month extension) all that had been planned originally for 36 months. In this project it has been necessary to develop techniques prior to acquiring hard data, so that cutting off the final year (or 9 months) has had consequences beyond merely reducing data production by one-third (or one-fourth). In spite of this cutoff, however, it has been feasible to generate useful results. And, the work will be continued so that all of the outputs originally planned will be generated somehow.

Acknowledgments - The members of the university team who have worked diligently to produce the technical results presented here have been Mr. Paul C. Power, Jr., Dr. Donald Sherman, Mr. Robert A. Wipf, Miss Marlene Witkowski, Mr. Frank Charnon, Mr. Karl Scheibengraber, Mr. Douglas Maercklein, and Mr. John Awald. We are also deeply grateful for the logistic and technical support of those personnel who have had no formal obligation to this project but who have cooperated unselfishly. Finally, we appreciate greatly the continuing cooperation of personnel of the U.S. Bureau of Mines.

Background and Previous Work

Progress in this project has been reported previously in detail in the semiannual technical report of August 26, 1971, the annual technical report of February 10, 1972, the semi-annual technical report of July 24, 1972, and in monthly and quarterly technical reports. Since much of the circulation of this current final report includes the same people circularized earlier in semiannual and annual reports, detailed technical information on procedures and equipment presented earlier will not be repeated here unless there have been revisions or the information is necessary to support the discussion.

The List of Referecnes Consulted (Appendix B) can provide the interested reader with background information and accounts of previous and related work.

Following is a brief narrative on background.

In recent years many data have become available on the mechanical behavior of rocks. It is clear that for all but very few rocks the classical models of isotropic, homogeneous, ideally elastic bodies are not valid. In the attempt to explain rationally the complex mechanical behavior of rocks, increasing attention has been given to identifying relationships between fabric and mechanical behavior.

Most fabric studies performed in the past have yielded results achieved only after very tedious work. Some analytical fabric studies include a subjective element that renders impractical the pooling of results based on work by different operators. The approach presented here provides the means to characterize deformation fabrics more objectively and efficiently.

The experimental techniques required to produce deformation suites of rocks for this study are well established or are modifications of established experimental procedures. Standard uniaxial loading and cantilever and third-part loading of rock slices cemented to aluminum beams have provided input data for spatial analysis by optical diffraction. Specifically, the input data consist of two-dimensional depictions of the rock fabric under load, where the fabric is recorded by conventional photography, photography in ultra-violet light of specimens treated with fluorescent dye penetrants, and photography of acetate peel replicas of specimen surfaces.

The optical diffraction method used in this project is based on work in 1873 by Abbe. With the appearance of the laser in 1960, it bacame practical to use this method for optical data processing.

The basic technique used is spectral analysis of the input's spatial frequency content by optical diffraction. The input is a reduced transparency that functions as a diffraction grating with unknown spatial properties. The source of illumination has precisely known spectral properties, i.e., it radiates coherent monochromatic light. The resulting diffraction pattern is the two-dimensional Fourier amplitude transform of the input image. This transform is a graph of the distribution of orientations and spacings of the elements in the input.

With additional optics the input image can be reconstructed from the light rays that form the diffraction pattern. A filtered, reconstructed image can be formed by blocking out some of the light rays in the plane of the transform. Such filtering can be used to suppress dominant alignments in the input so that obscure features can be detected more easily, and to aid in analyzing complicated distributions by systematically removing different components of the input. Through their diffraction patterns, orientation fabrics in rocks can be described, regardless of scale, in terms of spacings, directions, elongations, and symmetries. Changes in fabric associated with loading can be characterized through changes in transforms.

A limitation inherent in the optical diffraction method used here is that the inputs are two-dimensional. It is assumed, therefore, that what can be seen on the surfaces of specimens is significant in characterizing the deformation. We have systematically studied groups of specimens representing three mutually perpendicular orientations.

Another limitation in the project is that the observation of specimens under load has been restricted to deformation experiments without confining pressure. Fabrics of triaxially loaded specimens will be studied later, although at first the fabrics will probably be recorded following loading, not during loading.

Methods of Investigation

The methods of investigation used during most of the term of this project have been described in detail in our earlier semiannual and annual reports, and in papers cited in Appendix B.

The basic deformation experiments performed in this project and equipment configurations for accomplishing photography under load are shown in Figure 1.

The rock deformation experiments have consisted of uniaxial deformation of cylinders and prisms and cantilever and third-part loading of thin rock slices cemented to 10-1/8 x 2 x 1/4 in. (257.175 x 50.8 x 6.35 mm) aluminum beams. During deformation we have recorded changes in the two-dimensional fabric of the rock. Oriented samples have been cut from one foot cubes of St. Cloud Gray Granodiorite, Westerly Granite, Barre Granodiorite, Dresser basalt, Sioux Quartzite, Berea Sandstone, Tennessee marble and Salem Limestone, comprising the "ARPA suite."

The changes in fabric have been analyzed by optical diffraction analysis using operations and layouts illustrated in Figure 2. A Conductron LaserScan C120 System constitutes the core of the optical diffraction capability. High quality photographs and acetate peels are used to record the fabric at successively higher loads or strains. For photography, specimens are illuminated in white light, and in ultra-violet light after treatment with fluorescent dye penetrants. Figure 2 illustrates the layouts for photography. Figures 4-8 illustrate operations with acetate peels, which have turned out to be the most trouble-free procedure for recording fabrics.

Series of reference inputs and transforms have been prepared to provide bases for analyzing and comparing our experimentally generated data.

In addition to photographs of rocks undergoing deformation and peels taken from them we have also successfully produced transforms using thin sections as inputs and a petrographic microscope as an optical diffraction system. We have also done developmental work in holographic subtraction, in order to depict directly the changes between two inputs at successive stages of loading (Figure 3).

Technical Developments

An outline of technical developments, some of which have been described in earlier reports, is presented below:

1. Spatial filtering - Both directional and frequency filtering capabilities has been developed to provide all of the intensity filtering necessary for the work in this project. Suites of filters on film and glass plates, catalogues to select filters readily, and hardware to position the filters are all operational.

2. Mapping transforms - The mapping of transforms with spot-scanner and strip-chart recorder has been made a completely routine procedure. A portion of a profile of a calibration transform, using an input of rectangular coordinate paper, is presented in Figure 9, to show the quality profile available. A laser power meter, with sensitivities down to .0001 mW, has been acquired and modified to provide standardization of power levels among profiles to be compared.

3. Optical diffraction analysis of thin-sections - As part of this project, Power (1973) has successfully demonstrated the feasibility and practicality of generating transforms directly from thin sections of rocks with a research petrographic microscope. He has also demonstrated the superiority of this method for extracting some fabric data. The study also presents the theoretical bases for the conclusions drawn. In Figure 10 some of the experimental results obtained by Power are presented.

4. Production of reference inputs and transforms - Over 500 reference transforms and their inputs have been assembled to provide bases for analyzing experimental results. In Figure 11 we present a sample from this collection.

5. Preparation and deformation of rock slices - The study of strain distributions over the surface of rock slices cemented to aluminum bars has shown that the thickness of the glue line must be kept to .003 in. (.00762mm) or less. Under these circumstances, strains are proportional to load, are reproduced on unloading, and hold steady under load for 15 minutes. The proper glue thickness is obtained by curing under a clamp load of 20 lbs. (9.0718 kg.)

6. Photographic procedures - All photographic procedures, including preparation of inputs, darkroom work, and preparation of outputs have been standarized to insure consistency of results. In addition, a gray scale is photographed with each input series to provide the means for comparing inputs from different experiments. The university's senior photographer provided consultation and training during the development of these procedures. Capabilities for linear development and reversal processing were also achieved.

7. Study of closed curves (contours) - A paper by Pincus, Power, and Woodzick (1973 in press) on optical diffraction analysis of closed curves has been completed and accepted for publication by Geoforum. This work was partly supported by this project.

8. Study of particulate materials - A related project (Larson, 1973) supported by the U.S. Bureau of Mines but drawing on know-how generated in this project has generated results relevant to the objectives of this project. Shapes of particles, for example, have been shown to be amenable to optical diffraction analysis (Figure 12).

9. Improvement of acetate peel method - The use of acetate peels to record fabrics of specimens under load has been refined, both in terms of peel generation and photography of the peels for optical processing. In fact, the acetate peel method now appears to be the most reliable, trouble-free procedure we have used to record fabrics.

10. Work still in progress -

    a) Holographic subtraction - We have produced high quality image holograms and have achieved some success in subtracting one test input from another. A plexiglas enclosure has been constructed for isolating the optical system from vibration - generating air currents. A pneumatic system for isolating the system from floor vibrations is under construction, following completion of a vibration analysis of the bench, table, and floor.

    b) Construction of comparator - A comparator for determining quickly gross differences between similar transforms has been designed and all required equipment for construction is on hand. Construction will be started when feasible.

c) Analog processing of spot scanner profiles - Components have been received for construction of an analog system to provide square roots, integrals, and integrals of square roots of light intensities in profiles of diffraction patterns. The feasibility and desirability of performing these operations has been demonstrated using a borrowed computer. Construction is proceeding as this report is being written.

d) Third-part loading in tension - A fixture has been constructed and put into operation for tensional loading in a third-part configuration to permit recording of fabrics of rock slices under load, using the same recording procedures as for compressional third-part loading (Figure 4 and 5).

Implications of these technical developments are presented elsewhere in this report, as are advances in analytical techniques not explicitly presented in this section.

Technical Problems

Many of the technical developments listed in the preceding section were at one time technical problems that have been solved, bypassed, or mitigated. Earlier reports give accounts of such progress.

At this time there appear to be no major technical problems to report.

The apparatus to isolate the optical system from floor vibrations has to be built to facilitate holographic subtraction, but we have available to us the equipment configurations already used to solve this problem in other laboratories.

Occasional breakdowns of equipment have interfered with our progress, but the effects have been only delays at worst.

Administrative Problems

Changes in working assignments and in some key personnel in January 1973 decreased our production until the new arrangements were thoroughly assimilated.

As reported earlier, some of the vendors with whom we have had to deal have given less than satisfactory service. In recent months, as purchases tapered off, our dependence on promptness of deliveries decreased markedly.

Experimental Results and Interpretation

Introduction

The number and types of deformation tests conducted since the initiation of this project early in 1971 are shown in Table 1. Of the 211 tests, 131 have been conducted since the last semiannual technical report, July 24, 1972. Specimens have been prepared for an additional 134 tests, to be conducted as soon as adequate funding becomes available.

Of the 211 tests conducted so far, we have processed results from 137 tests at least through the transform stage of analysis and with sufficiently high standardization in all stages of production to permit valid cross-comparisons. Since transforms have been prepared for series of data points in each test, we have produced from the 137 tests about 800 transforms, with at least two standardized exposures per transform.

In addition to the 137 tests, results from over 20 additional tests are available, either as photocopies of acetate peels or as acetate peels not yet copied. Thus, the results of about 160 tests so far constitute the core of comparable data, representing close to 1000 data points on rock deformation.

Results from about 50 tests, conducted and processed early in the project, are also available. Those, however, are not standardized to be fully comparable to the results of the 160 tests. They have yielded useful data and constitute an informative reference source. Some of the 50 tests were also conducted for mechanical property data alone or to test out laboratory techniques; for these, useful fabric records are not typically available.

The totals cited in the foregoing paragraphs do not include the many results obtained from reference inputs and their transforms, thin-section inputs and their transforms obtained with the microscope, and analyses of closed curves (contours); all of these have been elucidated in earlier reports or are referred to or discussed elsewhere in this report.

In the past five months we have also produced 77 profiles of 36 transforms. When our analog processing capability is fully realized, the rate of producing profiles will also be increased because our capacity for interpreting them will be greatly increased. Some results based on analysis of about 2/3 of these profiles appear later in this section. Earlier reports presented profiles configured as spoke diagrams, a format we continue to believe is useful.

TABLE 1 - NUMBER AND TYPE OF DEFORMATION TESTS

	SLICES-CANTILEVER			SLICES - 3d PART			CYLINDERS				REMARKS
	R.I.	U.V.	A.P.	R.I.	U.V.	A.P.	R.I.	U.V.	A.P.		
BARRE GRANITE	6-T 3-C	6-T 3-C	6-T 3-C	3-T 6-C	2-T 4-C	3-T 6-C	7-C (7 ADD. CYLS. PREPARED)		9-C	67	2 PRISMS PREPARED
ST. CLOUD GRAY GRANODIORITE	6-T	1-T	6-T 3-C	3-T 6-C	3-T 6-C	3-T 6-C			3-C	46	
WESTERLY GRANITE			6-T 3-C	(12 ADD. SLICES PREPARED)		3-T 6-C	3-C (21 ADD. CYLS. PREPARED)		3-C	24	
DRESSER BASALT				(11 ADD. SLICES PREPARED)		3-T 3-C	(24 ADD. CYLS. PREPARED)		3-C	9	
SIOUX QUARTZITE				(3 ADD. SLICES PREPARED)		3-T 3-C	(CYLINDERS IN PREPARATION)			6	DRILLING DIFFICULT
BEREA SANDSTONE				(12 ADD. SLICES PREPARED)		3-T 3-C	3-C (21 ADD. CYLS. PREPARED)		3-C	12	
TENNESSEE MARBLE			6-T 3-C	(12 ADD. SLICES PREPARED)		3-T 6-C	6-C (10 ADD. CYLS. PREPARED)		9-C	33	
SALEM LIMESTONE				(5 ADD. SLICES PREPARED)		1-T	4-C (14 ADD. CYLS. PREPARED)		9-C	14	
	CANTILEVER TOTAL 61			3d PART TOTAL 88			CYLINDER TOTAL 62			211	

R.I. - REGULAR ILLUMINATION
U.V. - ULTRA-VIOLET ILLUMINATION WITH DYE PENETRANT
A.P. - ACETATE PEEL REPLICA (PHOTOCOPIED)
T - TENSION TEST
C - COMPRESSION TEST

R.I. TOTAL 56
U.V. TOTAL 25
A.P. TOTAL 130
GRAND TOTAL 211

We are not transmitting in this report the extremely large amount of data obtained in this project. Samples of results have been presented in earlier reports and samples of some additional results are presented here. Somehow, we will continue our analytical work during what had been planned as the third, ARPA-supported year: the project's "payoff" year. The transit time in this project for passage through the processing pipeline is such that many of the data did not become available until after ARPA support had ended and university support filled the gap; the data yield will continue to be large as operations continue.

Mechanical Property Testing

Regarding mechanical property testing, both cylinders and slices have proved to be quite practical for our purposes. We had hoped also to work with rock prisms but specimen production problems, now solved, did not leave adequate time for mass production of prisms. We still consider prisms to be worth studying and will do so when we can.

As the work in the project progressed, we changed our testing schedule to test more slices in compression and fewer in tension than had been planned originally. It was found also that the number of replicated experiments originally planned had to be decreased in order to stay within both time and funding constraints. Likewise, the number of specimens instrumented with strain gages was decreased to effect economies in time and funding. None of the foregoing changes has diminished the quality of our results, as far as we can tell; these changes have been simply part of the response to learning that takes place in any viable enterprise.

The mechanical property data obtained are reasonably consistent with results obtained in the Bureau of Mines in published and unpublished reports. However, our testing specimens in three mutually perpendicular directions have yielded additional evidence for mechanical anisotropy not evident from the extramural data available to us.

The ARPA suite of eight rocks provided us have presented an interesting variety of materials, but their mechanical testing has not yielded some of the types of deformation curves we have been seeking; we had hoped for some sharp breaks in slope, points of inflection, and the like. And, we had also hoped to find some useful regular reference shapes within the rocks to monitor in detail during deformation. The ARPA suite merits continuing study, but we intend to supplement these with rocks listed later under "Implications for Further Research."

The use of rock slices cemented to aluminum bars loaded as cantilevers and in third-part configuration presented some

interpretive problems. Following is part of an analysis developed to deal with these problems.

Strains in Rock Slices

Analysis of project data and an independent master's project have provided information on the stresses in the experiments with rock slices. As a result, modifications have been made in the procedure for preparing and mounting rock slices. The configuration of the slice specimen and the notation used to describe it are defined in Figure 13a. Also shown in Figure 13a are the general distribution of strain across the width and along the length of the slice.

Initial measurements in rock slices and an aluminum slice indicated as much as 15% strain variation across the width of the slice. A specimen with an aluminum slice integrally machined from the bar showed less than 2% variation, indicating that the larger variations were due to the bonding. Several bonding procedures and materials were studied and the results indicated that a thin glue line was desirable. The data in Table 2 are for an aluminum slice bonded with Epoxi-Patch 0151 under 20 pounds (89N) load resulting in a 0.003 inch (.0762 mm) glue thickness.

The data show:

1. Little or no strain variation across the width.
2. Good linearity
3. Reproducibility on unloading
4. No drift under sustained load and complete recovery on unloading.

Therefore, it was concluded that mounting rock slices with the Epoxi-Patch cured with a 20 pound (89N) spring clamp would eliminate any significant effect of the bond on the strain data.

The important factor involving the strain distribution along the length is the distance (β) from the edge at which the strain becomes uniform. Figure 13b summarizes the results of the three tests on integral aluminum slices. It is concluded that all data must be taken at a distance from the edge of the slice equal to 90% of the combined thickness of the slice and bar, or greater than 0.3 inches (7.62 mm) in this study.

Analytically the strain at the surface of the rock slice, ε_R, is a function of several factors:

TABLE 2 - Strains in Rock Slice

Specimen: Third part loading with aluminum slice

Bond: Epoxy-Patch 0151 cured under 20 lbs. (89N) load

Dimensions: Bar thickness - 0.251 in. (6.375 mm)
Slice thickness - 0.072 in. (1.829 mm)
Total thickness - 0.326 in. (8.280 mm)
Glue thickness - 0.003 in. (.0762 mm)

Load (Lb.)	Load (Kg)	Strain (μ in./in) Center	Strain (μ in./in) .75 in (19.05 mm) from ℄
0	0	0	0
40	18.14	190	185
80	36.29	380	370
120	54.43	560	560
160	72.58	745	745
200	90.72	930	930
160	72.58	745	745
120	54.43	560	560
80	36.29	377	372
40	18.14	190	187
0	0	0	0
0	0	0	0
200	90.72	930	932
200	90.72	930	932
(15 minutes)			
0	0	0	1

$$\frac{\varepsilon_R}{\varepsilon_o} = \frac{1 + 2(t/t_a) - (1 + t/t_a)(nb/b_a)(t/t_a)/\{1 + (nb/b_a)(t/t_a)\}}{1 + (nb/b_a)(t/t_a)^3 + 1/3(nb/b_a)(t/t_a)^3\{(1 + t/t_a)(t/t_a)\}^2/\{1 + (nb/b_a)t/t_a\}}$$

where $\varepsilon_o = \dfrac{6M}{E_a b_a t_a^2}$ (strain with no slice)

$n = E_R/E_a$

E_R = modulus of elasticity of rock

E_a = modulus of elasticity of aluminum

M = the bending moment

This equation is plotted in Figure 13c which illustrates that the strain is highly dependent on the rock modulus. The dependence on the slice thickness also varies with the rock properties. It was concluded that rather than spending the time to maintain a close tolerance on the slice thickness, which still results in a variable tolerance on strains, it would be more efficient to measure accurately the dimensions, obtain the nb/b_a parameter empirically, and make analytical corrections for the actual thickness. Even though the equation appears complex, results can easily be obtained by tables, graphs or computer reduction of data.

The foregoing analysis was carried out by Dr. Donald Sherman, Associate Professor of Engineering Mechanics at UWM.

Optical Diffraction Analysis

In the fabric records of rocks in deformation suites, we have been looking typically at spacings of 1 to 0.02 mm, with most of our attention in the range of 0.5 to 0.10 mm (2 to 10 lines/mm). Fabrics have typically been recorded and processed as inputs for diffraction analysis at a scale of 1:1.

A variation to be introduced definitely as soon as appropriate equipment can be purchased will be to produce routinely inputs at 10X magnification in addition to the 1X. Results to date indicate that the 1X scale is very definitely within a useful range for this work; we believe that we can obtain additional useful information, especially for rocks like the Salem Limestone, Berea Sandstone, and Dresser basalt with 10X inputs. It must be emphasized that a 10X enlargement of a 1X record is not nearly as useful as high-quality 10X photography.

Of the three techniques for recording fabrics in our rock deformation series, namely, regular illumination and photography, ultraviolet illumination of rock treated with fluorescent dye penetrants, and acetate peel replicas (photocopied at 1:1), the last has been the most effective and the second has been the least effective. The acetate peels do record fabric changes over a wide range of scales and they do not require the use of a camera and accessories during the deformation experiments. There is no depth of field problem or distortion in working with curved surfaces. The peels seem to work well with all of the eight rock types.

One difficulty we had earlier resulted from adhesion of particulate materials to the first peel applied (under no load); this was overcome by disposing of the first peel and applying a second peel under no load; this second peel is then the first peel of record. Another difficulty arises from bubbles under the peel; the bubbles account for high-frequency noise that can be misinterpreted. Even with very great care in applying the peels, one must guard against such misinterpretations by carefully examining the input photocopies, especially when the constrst between two transforms in a deformation series consists largely of more high frequency content in one.

The fluorescent dye penetrant works well in rocks with cracks but in rocks with much intergranular porosity the penetrant is fairly uniformly absorbed and adsorbed, leaving insufficient contrast in detail. There are also some special standardization problems here, in that is is very difficult to regulate the penetrant treatment from one specimen to the next with sufficient uniformity to permit interpretation of differences in transforms as resulting from

differences in fabric. The Salem Limestone and Berea Sandstone have not been effectively studied by penetrants.

Using regular illumination and photography, the main problem characterizing this method is in recording features in rocks with very low contrast. Increasing the intensity of illumination does not necessarily improve the situation, and in fact may seriously reduce comparability with other series of photographs. By trial and error we have arrived at a combination of parameters that permit overall reliable photography, however materials such as the Dresser basalt are not as efficiently studied as with acetate peels.

Operator error does seem to be a much smaller factor in working with peels than with either of the other two methods.

The type of deformation test used may be of some significance in producing and interpreting transforms. Where tension cracking is dominant the spatial frequency shift is toward lower values as cracks widen, and crucial information may be lost in the D.C. spot (zero frequency) unless special precautions are taken, such as expanding the transform or decreasing the intensity of the laser beam. Where shear fracturing is dominant, the spatial frequencies increase as new cracks develop and their diffraction products cluster directionally into bands; this may require shrinking the transform or increasing the intensity of the laser beam. These are but a few considerations in optimizing transform production and interpretation. Actually, we usually find it possible to generate many transforms without varying optical parameters.

Figure 14 illustrates one procedure for interpreting transforms. A particularly useful region of the profile is between the two second-order diffraction spikes, and within that range, the region between the first and second order spikes is most useful. This corresponds to spacings of 0.40-0.20 mm (or spatial frequencies of 2.5 - 5 lines/mm) in the inputs. Note that as the specimen goes from no-load to the first-loaded state (14b) to 14c)), the profile becomes smoother and the profile level in the region of the first-order spike diminishes. Going from the first- to the second-loaded state (14c) to 14d)) the profile level remains about the same, but the curve becomes rougher. These changes are consistent with the closing up of cracks under initial loading and the onset of new fractures with increasing loading. Profiles b), c), and d) are oriented parallel to the axis of the cylinder, which is also the direction of compression.

The foregoing discussion of Figure 14 is semiquantitative at best, but it is informative. Another such procedure for analyzing the frequency content is to filter the inputs differentially using arrays of spatial filters or variable

spatial filters, observing which features are filtered selectively by each filter configuration; this approach has been discussed in earlier reports which have included also information on our progress in constructing filter sets which we have continued to use. Still another semi-quantitative method of looking at spatial frequency content is to compare inputs and their transforms with reference inputs and their transforms like those shown in Figure 11; the assembly of these reference series has also been discussed in earlier reports. Some collections of inputs and transforms, although not specifically intended to serve as references in rock deformation studies, can be used quite effectively in some circumstances; Figure 12, for example, may be used in studying changes in grain shape in, say, metaquartzitic conglomerates. Finally, holographic subtraction, mentioned elsewhere in this report (Figure 3) and in others is a specialized, powerful tool for accomplishing filtering to achieve, among other things, the analysis of spatial frequency content.

The semi-quantitative methods described in the preceding paragraph have all yielded useful results either in this project or in the work of other investigators; they are or should be part of the standby analytical armamentarium of an optical diffraction analysis laboratory. Although they may not be mentioned in the technical findings of a report, they have often been used to help select other analytical methods that are mentioned. These methods are intermediate between more nearly qualitative and quantitative methods, which also have their place.

A useful, basic qualitative approach is to examine, only by eye, series of transforms and their respective inputs. Following are brief discussions of several examples of such examinations. Consider the data from third-part loading of Berea Sandstone in compression and in tension (P083-S-1C and P085-S-1T). In the compressional series, there appears to be very little change with loading, possibly a slight decrease in the high frequency. In the tensional series, there is a definite increase in spatial frequency with loading. At the highest loads in tension, fairly intense low frequencies appear; the inputs for these loads show the appearance of cracks in crude polygonal patterns which, in the aggregate, show no preferred orientation.

In the data from uniaxial loading of a cylinder of Barre Granite (K-026-A-1C), the transforms of the zero-load and highest-load inputs are not conspicuously different. It appears that there has been some shift from the former to the latter from both low frequency and high frequency to medium frequency; the shift from high frequency may be an artifact resulting from the presence of flaws in the acetate peel for the zero-load case. The biggest contrast comes about midway in the series with the appearance in the transform of intersecting diagonal bands generated by conjugate shears with

acute bisectrix parallel to the cylinder's axis; the input shows another system of apparent conjugate shears with acute bisectrix perpendicular to the cylinder's axis.

In the data from uniaxial loading of a cylinder of Dresser basalt (K060-B-3A) both the zero-load and highest load transforms and inputs (and their intermediates) show diagonal lineaments, but the diagonals are slightly more prominent in the loaded case.

In the data from unixial loading of a cylinder of Westerly Granite(K054-A-2C), the high frequency content increases with loading. The high frequency addition appears early in the loading series.

To avoid giving the impression that all such examinations yield evidence of fabric change with load, we cite the uniaxial loading of a cylinder of Salem Limestone (K021-L-1A). One must look long and hard before seeing what might be slight but real changes in high frequency content. However, at 1/2 second exposure the zero-load transform seems to have slightly more high frequency content and at 1 second exposure the highest-load transform seems to have more high frequency content. This is the type of result that stimulates the search for more quantitative approaches, such as that presented later, and it also reinforces the need for caution in interpreting all results of this type of examination.

It appears from results like those discussed here and from results yet to be presented that fabric changes as detected in this study are less associated with elastic moduli, shapes of loading curves, and compressive strength than with initial fabric (both scalar and vector), contrasting physical properties of structural units such as grains and clumps of grains, mode of deformation, and the like. However, some fabric changes may prove to be useful indicators pointing to the likelihood of imminent failure. Further analysis of transforms and inputs on hand will shed more light on those relationships.

Interpretation of transforms and their inputs on either a qualitative or quantitative basis requires a systematic classification of transform properties. Figure 15, supplemented by Figure 16, presents such an approach. It must be emphasized here that we do not present this as our final word on classification and analysis: far from it.

The two basic changes (or contrasts) in transform properties shown in Figure 15 are spatial frequency and direction which are, after all, the two basic variables depicted in the transform. In Figure 15 the changes in these two variables are independent; in Figure 16 these changes are mutually dependent, that is, a change in one is related to a change in the other. Figures 15 and 16 exemplify changes or contrasts

and their combinations; they do not purport to be complete pictures of all variations. In fact, the body of Figure 15 shows only five examples of mutually independent combinations of changes. However, all of the transforms studied in this project can be plugged into Figures 15 or 16 or some variation of them.

These changes can be translated into fabric changes in rocks, and vice versa. For example, the extreme left example in the body of Figure 15 (combination of Change in Spatial Frequency (1) (b) and Change in Direction IV) could result from the compression of cracks (the narrower cracks being more compressed and even closed) and the generation of new cracks in a narrow range of directions. The translation of these changes into the equivalent conventional notation of petrofabrics is a task yet to be undertaken.

In Figure 16 C, for example, we see what could be the result of compression, elongation, and rotation (or recrystallization) of grains that originally had no preferred orientation or no elongation and the sizes of which initially varied continuously over the range of grain sizes.

From our studies, the fabric elements most commonly identifiable with transform characteristics are cracks (width, orientation, spacing), twinning and cleavage, grain boundaries, clumps of grains, banding (bedding, foliation), and veinlets. Any of these may lead to failure through mechanisms such as crack generation or growth.

It appears now the the purposes of one of our original objectives, namely, to establish a catalogue of standardized transforms, can be better served by the more flexible approach of using a classification such as that in Figure 15 in conjunction with the reference transforms and inputs already compiled to characterize and analyze real transforms and their inputs. The latter approach provides at least as much insight as the former and provides an infinite variety of approaches to transform analysis instead of a discrete, pigeonhole approach. One could, of course, also regard the sketches in Figures 15 and 16 as standardized transforms, but this could detract from their effective use if they are treated as pigeonholes.

To approach the analysis of transforms quantitatively, the thinking inherent in Figures 15 and 16 can be used in conjunction with some instrumented mapping technique. Figure 17 shows some desirable conventions for mapping transforms by profiling. The procedure in row D is equivalent to that used in preparing the spoke diagrams presented in earlier reports.

To proceed futher along the quantitative route, we have devised procedures, which, at the outset, must be clearly understood to be subject to further extensive testing and refinement. Figure 18 represents the graphical aspects of this approach.

First note the similarity between Figure 18 a) and Figure 14, and recall the discussion of Figure 14. In Figure 18 a), we have smoothed the profile in the region of the first and second-order diffraction spikes. The a-curve is the straight-line connecting the ordinates of the smoothed curve at the positions of the first and second-order diffraction spikes, for the transform at load a. The b-curve serves the same purpose for the transform at load b.

Figure 18 b) shows the change from an a-curve to a b-curve where the area beneath each from zero-frequency to the x-intercept is a constant; this conservation of area (actually total spatial frequency in this interval) is not required for what follows, but it is useful analytically to determine whether this area is indeed conserved, say in a deformation series. (The area would not be conserved, for example, where twinning or cleavage develops in calcite grains as observed in our experiments with Tennesse marble; this adds a high frequency component to spatial frequencies already present.)

We then proceed to construct some indexes based on the profile in the interval (I) between the first and second order diffraction spikes.

The relative change in area from the a-curve to the b-curve over the I interval is:

$$\overline{\triangle A} = \frac{1/2\,(\bar{a}_1 + \bar{a}_2)(I) - 1/2\,(\bar{b}_1 + \bar{b}_2)(I)}{1/2\,(\bar{a}_1 + \bar{a}_2)(I)}$$

$$\text{or } \overline{\triangle A} = 1 - \frac{\bar{b}_1 + \bar{b}_2}{\bar{a}_1 + \bar{a}_2}$$

where $\bar{a}_1 = 1/2\,(a_1 + a_1')$, $\bar{b}_1 = 1/2\,(b_1 + b_1')$, etc.

Reading errors for small values of b or a can be minimized by extending the b and a curves, reading the intercepts on the x and y axes, and calculating the b and a values at the first and second order spikes.

When $\bar{b}_1 \gg \bar{b}_2$ and $\bar{a}_1 \gg \bar{a}_2$,

$$\overline{\Delta A} \approx 1 - \frac{\bar{b}_1}{\bar{a}_1} .$$

When $\overline{\Delta A} > 0$, there is a decrease in area over I.

$\overline{\Delta A} = 0$, there is no change in area over I.

$\overline{\Delta A} < 0$, there is an increase in area over I .

In Figure 18 b), $\overline{\Delta A} = +0.46$. In this example, areas are conserved. The shift in spatial frequencies is toward higher values (+).

The relative change in slope from the a-curve to the b-curve is

$$\overline{\Delta S} = \frac{\{(\bar{a}_1 - \bar{a}_2)/I\} - \{(\bar{b}_1 - \bar{b}_2)/I\}}{(\bar{a}_1 - \bar{a}_2)/I}$$

$$\text{or } \overline{\Delta S} = 1 - \frac{\bar{b}_1 - \bar{b}_2}{\bar{a}_1 - \bar{a}_2}$$

When $\bar{b}_1 \gg \bar{b}_2$ and $\bar{a}_1 \gg \bar{a}_2$,

$\overline{\Delta S} \approx 1 - \frac{\bar{b}_1}{\bar{a}_1}$, which is also the approximate value for $\overline{\Delta A}$

under the same conditions. We introduce the notation

$$\overline{\Delta M} = 1 - \frac{\bar{b}_1}{\bar{a}_1}$$

to identify this expression.

In Figure 18 b), $S = +0.84$ and $M = +0.52$.

When $\overline{\Delta S} > 0$, there is a decrease in slope over I.

$\overline{\Delta S} = 0$, there is no change in slope over I.

$\overline{\Delta S} < 0$, there is an increase in slope over I.

A positive value of $\overline{\Delta M}$ means a decrease in the first order coordinate; a negative value of $\overline{\Delta M}$ means an increase in the first order coordinate.

Finally, Figure 18 (c) presents the basis for an index based on change in roughness or heterogeneity of transform profiles. Here, we work in the interval between the D.C. spike (zero frequency) and the first order spike. The index here is defined as

$$\overline{\Delta R} = \frac{\bar{r}_a - \bar{r}_b}{\bar{r}_a}$$

$$\text{or } \overline{\Delta R} = 1 - \frac{\bar{r}_b}{\bar{r}_a} .$$

r_a = number of spikes between D.C. (zero frequency) and the first order spike with height $\geq$ some constant, specified fraction of the height of the first order spike, for load a.

r_b = same as for r_a , for load b.

$\bar{r}_a$ = mean value of r_a for both sides of the profile.

$\bar{r}_b$ = mean value of r_b for both sides of the profile.

In Figure 18 c), the constant fractional value of the first order spike is taken at 0.1, and $\overline{\Delta R} = +0.75$.

In our work in this project, the constant fractional value actually used is 10^{-5}, because several scale changes are necessary to chart spike amplitudes for the very intense calibration transform profile and the transform profiles of the rock fabrics studied. All of the transforms of rock fabrics are run with identical instrumental and optical settings.

When $\overline{\triangle R} > 0$, there is a transition to a smoother profile.

$\overline{\triangle R} = 0$, there is no change in roughness.

$\overline{\triangle R} < 0$, there is a transition to a rougher profile.

Changes in magnitude but not sign of any of these indexes is easily interpreted. For example, suppose that in a deformation series we calculate a $\overline{\triangle R}$ for the first loading point with respect to zero load and find it to be positive. Then suppose that we calculate the $\overline{\triangle R}$ for the second loading point with respect to zero load and find it also to be positive but smaller than the first $\overline{\triangle R}$. This means that the transform profile becomes smoother from zero load to first load and less smooth from the first load to the second.

Tables 3 and 4 illustrate the applications of $\overline{\triangle A}$, $\overline{\triangle S}$, $\overline{\triangle M}$, and $\overline{\triangle R}$ to a variety of experiments and orientations, all for Tennessee marble. Any of the four indexes becomes an index of deformation in terms of fabric change or an index of fabric heterogeneity, depending on where and how it is applied.

For a particular type of experiment, the same rock type, the same specimen orientation, and the same profile orientation, the changes noted are functions only of loading (Indexes of deformation).

For a particular type of experiment, the same rock type, the same profile orientation, no load, and different specimen orientations, the changes noted are functions only of specimen orientation (Indexes of fabric heterogeneity). If we then look at the indexes for equivalently loaded specimens, we see the effects of interactions between loading and orientation.

For profiles in different directions with all other factors the same, we are looking at variations in fabric in a particular surface (Indexes of fabric heterogeneity in a surface).

There are many ways of looking at these data, and we leave it to the reader to explore as he sees fit.

Some of our results are to be expected, and others are unexpected. Specimen orientation in some cases appears to be very important in terms of deformation, and may be related to foliation and to measured differences in elastic moduli. But in other cases, deformation seems to wipe out fabric differences observed at no load.

Changes in fabric seem, in some cases, to occur without any clear association with progressive loading (or strain); that is neither the mode of fabric change is persistent nor

Table 3 - Examples of data analysis
Cylinder experiments

TENNESSEE MARBLE, UNIAXIAL LOADING-CYL. ACETATE PEEL.

A.- CHANGE IN LOAD

	Load	$\overline{\Delta A}$	$\overline{\Delta S}$	$\overline{\Delta M}$	$\overline{\Delta R}$
Specimen orientation #2. Profiles parallel to cyl. axis. ("90° profile")	a, c	+0.47	+0.57	+0.52	+0.67
	a, e	+0.44	+0.45	+0.44	+0.39
Specimen orientation #2. Profiles perpendicular to cyl. axis. ("0° profile")	a, c	+0.58	+0.66	+0.61	+0.47
	a, e	+0.67	+0.63	+0.65	+0.41
Specimen orientation #2. Comparison of parallel and perpendicular profiles at equal loads	a	0	+0.31	+0.15	+0.06
	c	+0.20	+0.45	+0.31	-0.50
	e	+0.41	+0.54	+0.47	+0.09
Specimen orientation #3. Profiles parallel to cyl. axis	a, c	-0.60	-0.57	-0.58	-0.10
	a, e	-0.73	-0.50	-0.625	-0.20
Specimen orientation #3. Profiles perpendicular to cyl. axis.	a, c	-0.22	-0.21	-0.22	+0.27
	a, e	-0.30	-0.21	-0.26	+0.27
Specimen orientation #3. Comparison of parallel and perpendicular profiles at equal loads.	a	-0.04	+0.14	+0.04	-0.10
	c	+0.20	+0.33	+0.26	+0.27
	e	+0.22	+0.30	+0.26	+0.33

	p.s.i.	MN/m²
a	0	0
c	7220	49.8
e	13540	93.3
g	16250	112.0

(continued)

	Load	$\overline{\Delta A}$	$\overline{\Delta S}$	$\overline{\Delta M}$	$\overline{\Delta R}$
Specimen orientation #1. Profiles parallel to cyl. axis ("90° profile.")	a, c	-0.07	-0.09	-0.08	-0.22
	a, e	+0.20	+0.27	+0.23	+0.11
	a, g	-0.13	0	-0.08	-0.33
Specimen orientation #1. Profiles inclined 30° from cyl. axis ("60° profile")	a, g	-0.07	-0.12	-0.09	+0.10
Specimen orientation #1. Profiles inclined 60° from cyl. axis ("30° profile")	a, g	-0.13	-0.33	-0.21	+0.09
Specimen orientation #1. Profiles perpendicular to cyl. axis ("0° profile")	a, c	-0.08	-0.125	-0.10	+0.08
	a, e	+0.08	+0.375	+0.20	+0.25
	a, g	-0.125	+0.06	-0.05	0
Specimen orientation #1. Comparison of profiles of different orientation at equal loads.	a, 90°, 60°	+0.10	+0.23	+0.15	-0.11
	a, 90°, 30°	+0.23	+0.32	+0.27	-0.22
	a, 90°, 0°	+0.20	+0.27	+0.23	-0.33
	c, 90°, 0°	+0.19	+0.25	+0.21	0
	e, 90°, 0°	+0.08	+0.37	+0.20	-0.125
	g, 90°, 60°	+0.15	+0.14	+0.14	+0.25
	g, 90°, 30°	+0.24	+0.09	+0.18	+0.17
	g, 90°, 0°	+0.21	+0.32	+0.25	0

(continued)

3.- CHANGE IN SPECIMEN ORIENTATION

LOAD PROFILE	ORIENTATION		$\overline{\Delta A}$	$\overline{\Delta S}$	$\overline{\Delta M}$	$\overline{\Delta R}$
Unloaded specimen.	a	90° 2 3	+0.54	+0.57	+0.56	+0.44
		0° 2 3	+0.53	+0.46	+0.50	+0.35
		90° 2 1	+0.47	+0.57	+0.52	+0.50
		0° 2 1	+0.58	+0.54	+0.57	+0.29
		90° 3 1	−0.15	0	−0.08	+0.10
		0° 3 1	+0.11	+0.15	+0.13	−0.10
Loaded specimen.	e	90° 2 3	−0.41	−0.18	−0.30	−0.09
		0° 2 3	−0.84	−0.77	−0.82	+0.20
		90° 2 1	+0.25	+0.43	+0.33	+0.27
		0° 2 1	−0.16	+0.23	0	+0.10
		90° 3 1	+0.47	+0.52	+0.49	+0.33
		0° 3 1	+0.37	+0.57	+0.45	−0.125

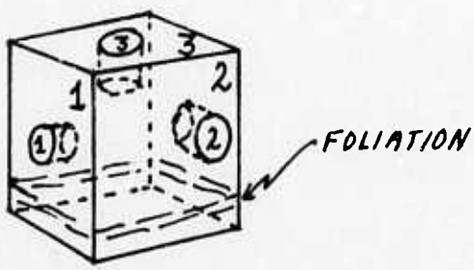

Table 4 - Examples of data analysis- Cantilever experiments

TENNESSEE MARBLE
CANTILEVER LOADING-SLICES
ACETATE PEEL
T- TENSION
C- COMPRESSION

A.- CHANGE IN LOAD

	Load		$\overline{\Delta A}$	$\overline{\Delta S}$	$\overline{\Delta M}$	$\overline{\Delta R}$	END-LOAD LB.	END-LOAD N
Specimen orientation #1. Profiles perpendicular to long axis of cantilever (90° profile)	a	T	-0.52	-0.17	-0.38	-0.29	a 0	0
	g						g 120	534
	a	C	-1.36	-1.29	-1.33	-1.50		
	g							
Specimen orientation #1. Profiles parallel to long axis of cantilever (0° profile)	a	T	-2.125	-3.25	-2.50	-3.00		
	g							
	a	C	-2.00	-2.00	-2.00	-0.60		
	g							
Specimen orientation #1. Comparison of parallel and perpendicular profiles at equal loads.	a	T	+0.45	+0.67	+0.54	+0.71		
	g		-0.14	-0.21	-0.17	+0.11		
	a	C	+0.18	+0.29	+0.22	-0.25		
	g		-0.04	+0.06	0	+0.20		
Specimen orientation #1. 0° profiles. Comparison of tension and compression at equal loads.	a		-0.125	-0.25	-0.16	-1.50		
	g	T,C	-0.08	+0.12	0	0		
Specimen orientation # 2. Profiles perp. to long axis of cant. (90° profiles)	a	T	-1.08	-0.73	-0.82	-0.125		
	g							
	a	C	-0.46	-0.35	-0.42	+0.20		
	g							
Specimen orientation # 2. Profiles parallel to long axis of cantilever. (0° profile)	a	T	-1.10	-1.33	-1.25	-3.00		
	g							
	a	C	-1.67	-2.60	-2.00	-1.20		
	g							
Specimen orientation #2. Comparison of parallel and perpendicular profiles at equal loads.	a	T	+0.23	+0.45	+0.33	+0.75		
	g		+0.22	+0.26	+0.22	+0.11		
	a	C	+0.36	+0.50	+0.42	+0.50		
	g		-0.17	-0.33	-0.23	-0.375		
Specimen orientation #2. 0° profiles. Comparison of tension and compression, equal loads.	a		+0.10	+0.17	+0.125	-1.50		
	g	T,C	-0.14	-0.29	-0.17	-0.375		

(continued)

	Load		$\overline{\Delta A}$	$\overline{\Delta S}$	$\overline{\Delta M}$	$\overline{\Delta R}$
Specimen orientation #3. 90° profiles.	a	T	+0.06	−0.33	−0.08	+0.10
	g					
	a	C	−4.56	−4.42	−4.50	−1.00
	g					
Specimen orientation #3. 0° profiles	a	T	+0.06	+0.08	+0.07	+0.20
	g					
	a	C	−2.17	−2.25	−2.20	−1.40
	g					
Specimen orientation #3. Comparison of parallel and perpendicular profiles at equal loads.	a	T	−0.06	−0.33	−0.15	0
	g		−0.06	+0.08	0	+0.11
	a	C	−0.33	−0.14	−0.25	+0.17
	g		+0.24	+0.32	+0.27	0
Specimen orientation #3. 0° profiles. Comparison of tension and compression, equal loads.	a		+0.67	+0.67	+0.67	+0.50
	g	T,C	−0.12	−0.18	−0.14	−0.50

B.- CHANGE IN SPECIMEN ORIENTATION

	Load	Orientation	$\overline{\Delta A}$	$\overline{\Delta S}$	$\overline{\Delta M}$	$\overline{\Delta R}$
0° profiles. Tension.	a	2	+0.20	+0.33	+0.25	0
		1				
		2	−0.80	−1.00	−0.875	−3.0
		3				
	g	2	−0.19	−0.21	−0.17	0
		1				
		2	+0.19	+0.21	+0.22	0
		3				
0° profiles. Compression	a	2	0	0	0	0
		1				
		2	+0.33	+0.20	+0.29	0
		3				
	g	2	−0.125	+0.17	0	+0.27
		1				
		2	+0.21	+0.28	+0.24	−0.09
		3				

is progress of fabric change uniform or continuous. All of these results, of course, need checking, refinement, and much more application.

The calculation of these indexes can be greatly improved. First, the use of the analog processor will greatly simplify work with the transform profiles and make the results more reliable through objective smoothing of the data. Second, digital processing of the profiles would greatly improve the quality of the results; this would also make it relatively simple to use measures that apply to larger portions of the transform, and to look for cross-correlations that would otherwise be too time-consuming to calculate.

Comparison of results from different types of tests will need to be interpreted with caution. A particular load level under tension may have carried a specimen well beyond failure while the same load level in compression has the specimen no where near failure. Also, our calculations show that the same beam load applied to cantilevers carries the stress level in rock slices far higher than in third-part loading and further, there is a stress gradient in cantilevers not operative in third-part loading.

However, the results so far seem to provide a substantial start on the index problem and do meet the project's objectives of generating indexes of fabric heterogeneity and deformation. During the months immediately ahead we will proceed along these lines, applying these methods to the large amount of data already on hand. As data are generated from the addicional tests yet to be performed, they will also be subjected to this type of analysis; this will necessarily come later than analysis of transforms and inputs already on hand.

Conclusions

The following general statements summarize our results:

1) Replicated experiments usually yield similar results.

2) Some results appear to be clearly dependent on orientation of specimens.

3) Within each class of experiment, the results are in general consistent with what is to be expected in classical tension (or extension) and compression experiments.

4) Decreases in spatial frequency with loading usually signify widening of cracks or other discontinuities.

5) Increases in spatial frequency with loading usually signify development of additional cracks or other discontinuities.

6) In a single specimen, the change of spatial frequencies may change signs during a loading experiment. The mode of fabric change may also change during loading.

7) The most profound changes in fabric, in terms of spatial frequencies determined by the methods presented here, may come just prior to failure, during failure, and following failure. However, we have found instances in which the most profound changes came at early-intermediate stages of deformation.

8) Unloaded specimens do appear to have different spatial frequency content from the same specimens before loading.

9) Initial fabrics may have a strong influence on subsequent deformation fabrics. However, loading may induce fabric changes that override initial fabrics.

10) Scalar fabric features, such as grain-size, may also profoundly influence deformation fabric.

11) The several indexes developed in this study appear to be promising, but need further testing and study.

12) The scale at which fabric has been mapped does reveal changes of significance with loading; scales at higher magnification should now be investigated.

13) Cracks (width, orientation, spacing), twinning, cleavage, grain boundaries, clumps of grains, banding, and veinlets are fabric elements most commonly identifiable with transform characteristics.

14) The acetate peel method for recording fabric appears to be the most reliable, trouble-free method of all those used.

15) The production of transforms directly from thin-sections with a research microscope has been demonstrated to be practical.

16) At this point, there do not seem to be simple and obvious relationships between the fabric elements studied and elastic moduli, shapes of deformation curves, and compressive strength. However, some fabric changes may prove to be useful indicators pointing to the likelihood of imminent failure and could be used for monitoring rocks in active excavations. Further analysis of the large amount of data on hand and of additional data to be generated will shed more light on these points.

Implications for Further Research

The technical results achieved in this project indicate that the methods used are sound and merit further application to other rocks. Rocks being considered for study in the future are:

Colorado oil shale (Green River)
Lithonia granite gneiss
Martinsburg slate
Yule marble
Baraboo quartzite
Funzie conglomerate

Possibly also cylinders and prisms from the ARPA suite have saw-cuts in varying orientations.

In addition, it is desirable to compare fabrics in experimentally deformed rocks with those in several selected similar rocks that failed under field conditions. Field localities being considered for such study are:

South Mountain Fold, Maryland
Rock Springs, Devil's Lake, and Baraboo, Wisconsin
Barberton Limestone Mine, Ohio
A cryptovolcanic structure (Indiana, Ohio, Tennessee, Ontario)
A block-caving mine (Climax, Col.; San Manuel, Ariz.)
One or two tunnels constructed for civil engineering purposes (Milwaukee, Minneapolis, Swiss Alps)

The routine application of holographic subtraction, in addition to the methods already developed and refined in this project, will undoubtedly help greatly in further characterizing deformation modes and intensities and in increasing our understanding of mechanical anisotropy.

As this research continues, we will obtain data on changes in fabrics of triaxially deformed specimens. This will be done by carrying cylindrical specimens to specified axial and radial loads and photographs will be made following unloading. Subsequently, we will obtain data from specimens under triaxial load.

As the research continues, we will also begin some pilot experiments leading to the capability of generating transforms in reflected light. Having demonstrated that slight changes in fabric are detectable by our techniques, we will investigate possibilities for in situ optical monitoring of rock fabrics in active excavations.

Special Comments

Related research projects in which we have been involved are providing materials and know-how of benefit to the conduct of this project, and vice versa. Those projects include a study of the effects of rock alteration, joint fillings, and fracture geometry on mechanical behavior of rocks, especially from block-caving operations. We are also measuring triaxial-acoustic properties of rocks from block-caving areas. Fabric analysis is an important aspect of these studies. We have also studied the transforms of separated particles of different shapes and sizes to determine empirically the effects of different configurations, shapes, spacings, and sample size; this work is also in the realm of research in mechanical behavior of rocks, for it is directed toward relating particle parameters to fragmentation history (Larson, 1973).

The study by Power (1973) on optical diffraction analysis of thin sections with a microscope provides the means for many laboratories to undertake spatial frequency studies of micro-fabrics with very little additional expenditure of funds. This is certainly one of the most important advances achieved in this project.

Concluding Remarks

Since this project has been supported for two-thirds of its projected life under the aegis of ARPA's Rapid Excavation Program, it seems wise to conclude with some brief comments on foreseeable benefits for rapid excavation.

The project has not been concerned with developing the hardware for rapid excavation. This project has been concerned with increasing understanding of some aspects of rock failure, and in the course of doing that, of developing techniques for studying fabric changes under load. In terms of both technical procedures and substantive information, advances have been made.

Further, an outcome of this work, fabric studies of thin sections directly with a microscope are now feasible via Fourier optics. And, we are not far from developing a reflection technique that could be applied in situ to monitor fabric changes in the surface of excavation or in boreholes.

All of these advances are applicable to both improvement in causing desired failure, that is in excavating, and improvement in preventing or mitigating failure, that is in maintaining or improving stability in excavations.

The follow-up work to be undertaken in the next year or two is expected to yield substantial pay-offs. For both future and present pay-offs and the opportunity to effect them we are grateful to ARPA and the U.S. Bureau of Mines.

Appendixes

A - Figures Accompanying Text

B - List of References Consulted

C - New or Modified Procedures and Lists

D - Distribution List

E - Form DD 1473 (Abstract)

APPENDIX A

FIGURES ACCOMPANYING TEXT

(List of Illustrations follows Table of Contents)

(a) Set-up for photographing rock slices tested in tension in cantilever loading apparatus.

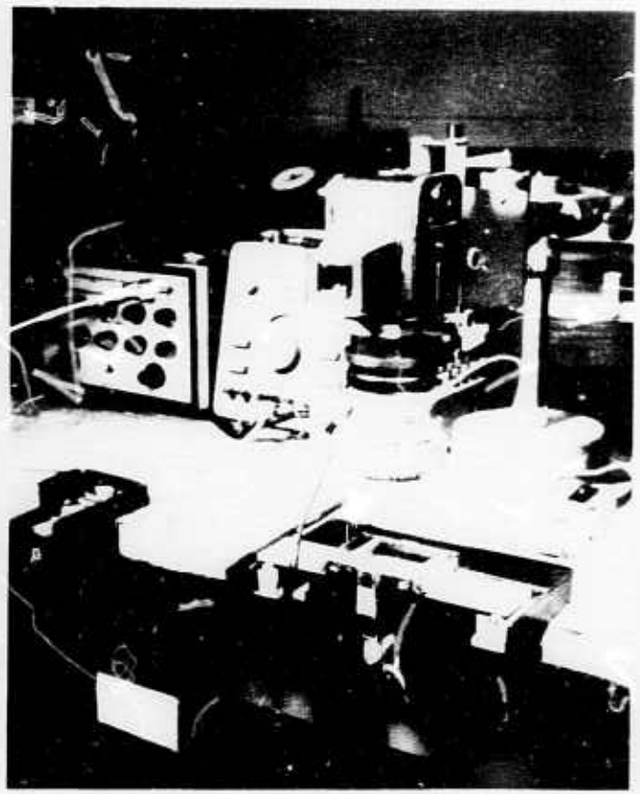

(b) Set-up for photographing rock slices tested in compression in third-part loading apparatus.

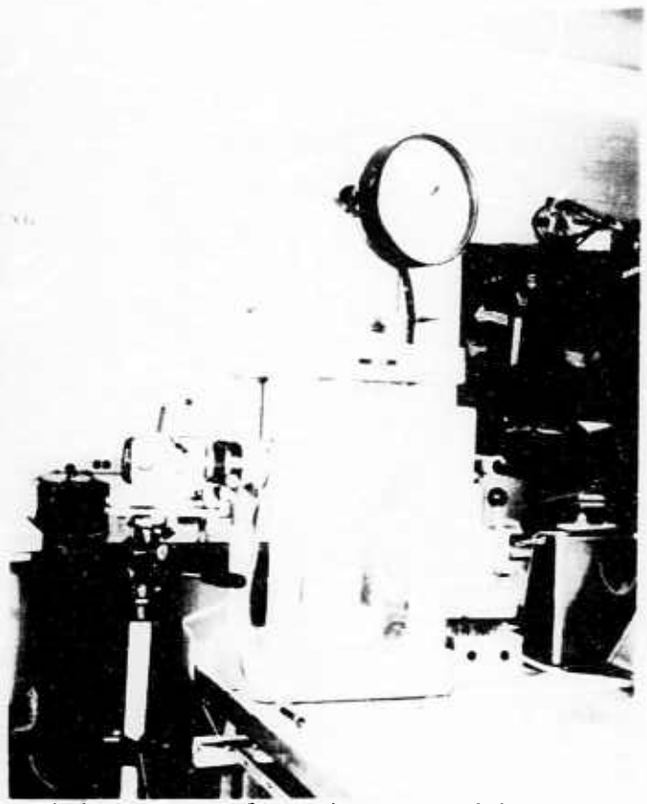

(c) Set-up for photographing rock cylinders tested in uniaxial compression. Plexiglas safety shield obscures specimen. The same set-up is used for testing prisms.

Figure 1 - Basic deformation experiments performed in this project and equipment configurations for accomplishing photography of specimens under load.

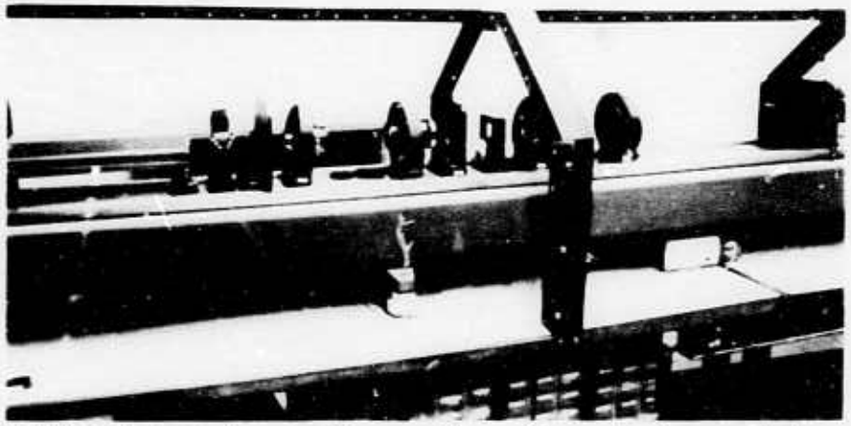

a) Optical bench configuration for photographing the transforms. Laser is at left and camera is at right

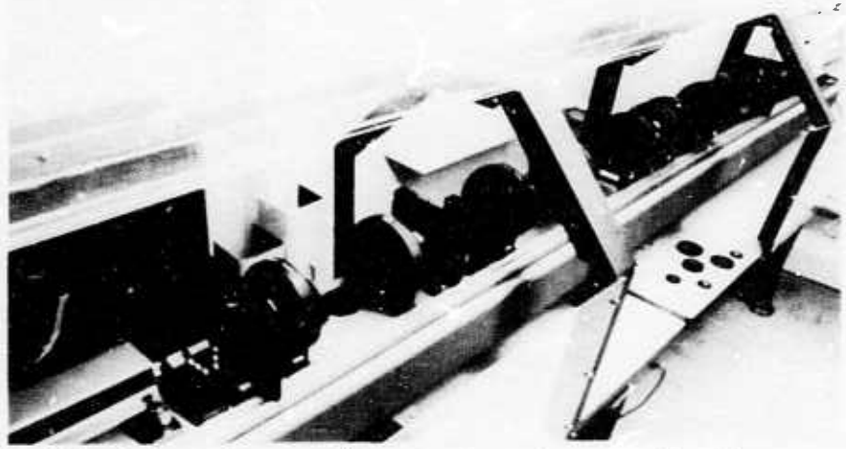

b) Optical bench configuration for real-time production of reconstructed filtered images. Laser is at lower left and TV camera is at upper right. TV monitor screen is shown on top shelf in c) on this page.

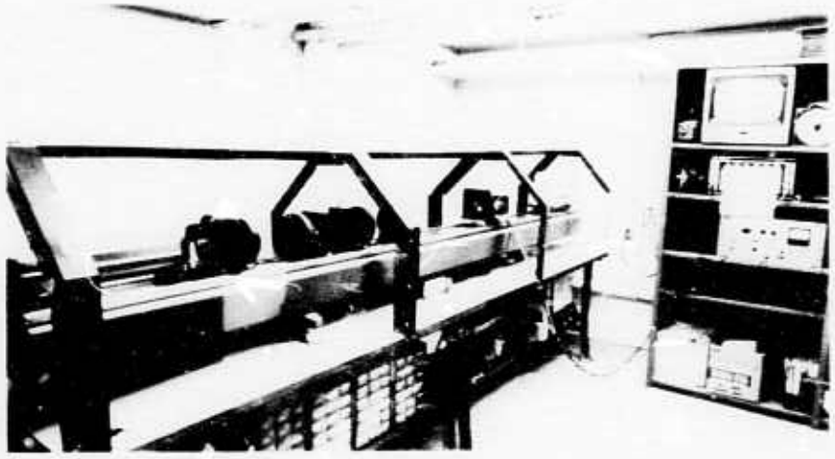

c) Set-up used for producing an intensity profile of the transform. The output of the scanning photomultipher (shown in detail in d)) is recorded on the strip chart at the right, second shelf from the top.

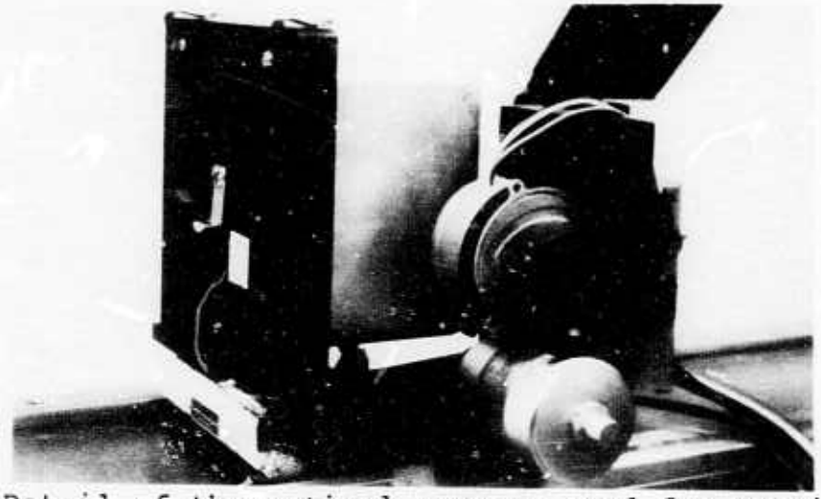

d) Detail of the optical scanner used for mapping transforms. Pin-hole is just below the J-shaped bracket on the black face-plate.

Figure 2 - Basic optical diffraction analysis operations and equipment lay-outs

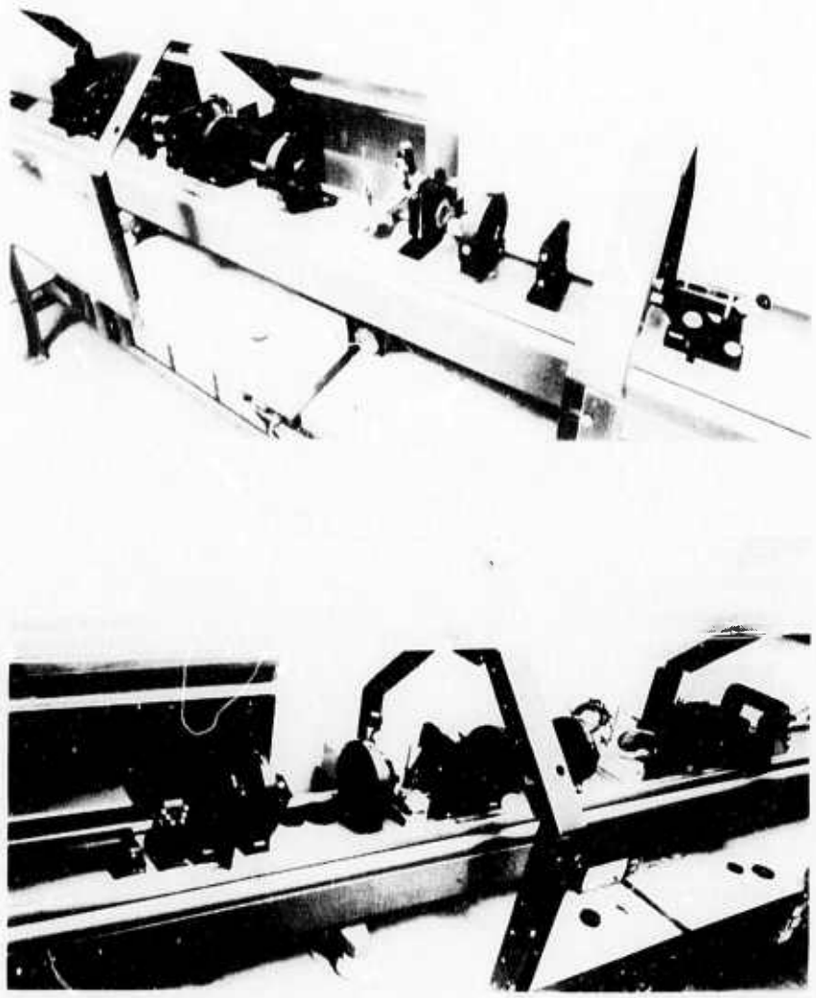

Figure 3 - Two views of the optical bench configuration for performing holographic subtraction. The plexiglas enclosure isolates the system from air currents. The two aluminum outriggers, each equipped with beamsplitter and mirror, provide a reference beam path outboard and on the far side of the optical bench.

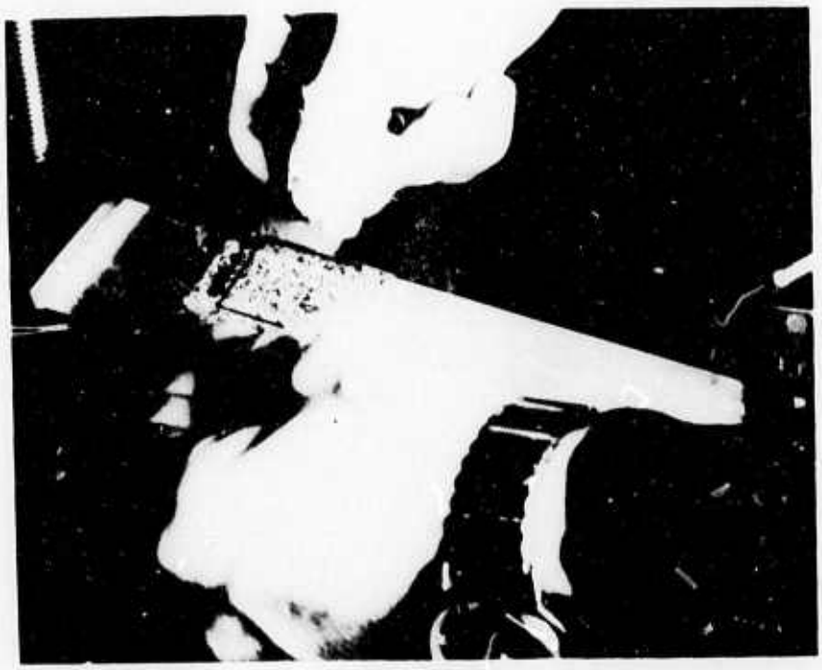

Figure 4 - Acetate peel being applied to rock slice loaded in tension in cantilever apparatus. Peel is bent downward, first contacting acetone at center of slice, to expel air bubbles. (See Figure 5b) for method of removing peel.)

a) Acetate peel being applied to rock slice in third-part tensional loading apparatus.

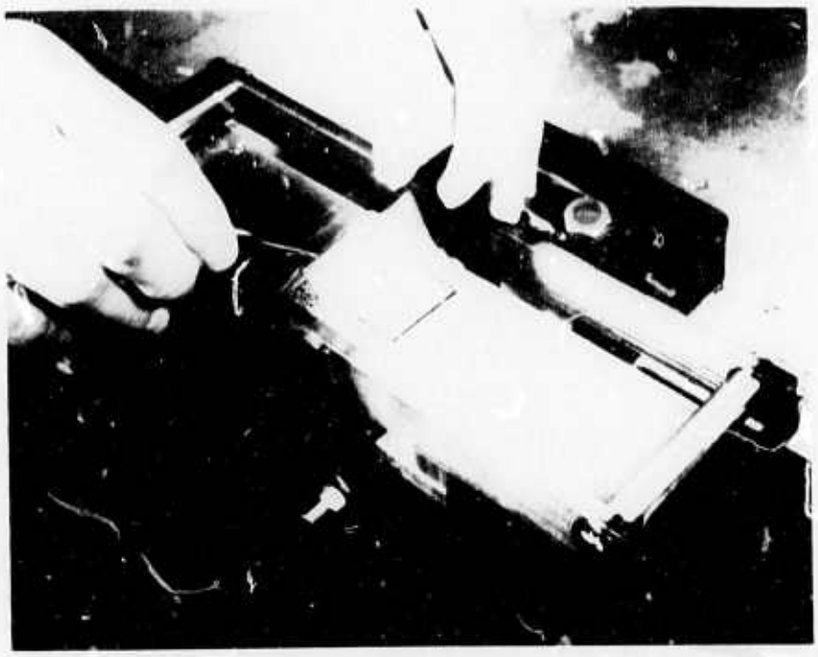

b) Acetate peel being removed from slice. Outside of peel is lifted and peeled gently and steadily toward the other to avoid folds and tears.

Figure 5 - Application and removal of acetate peel in third-part tensional loading of rock slice.

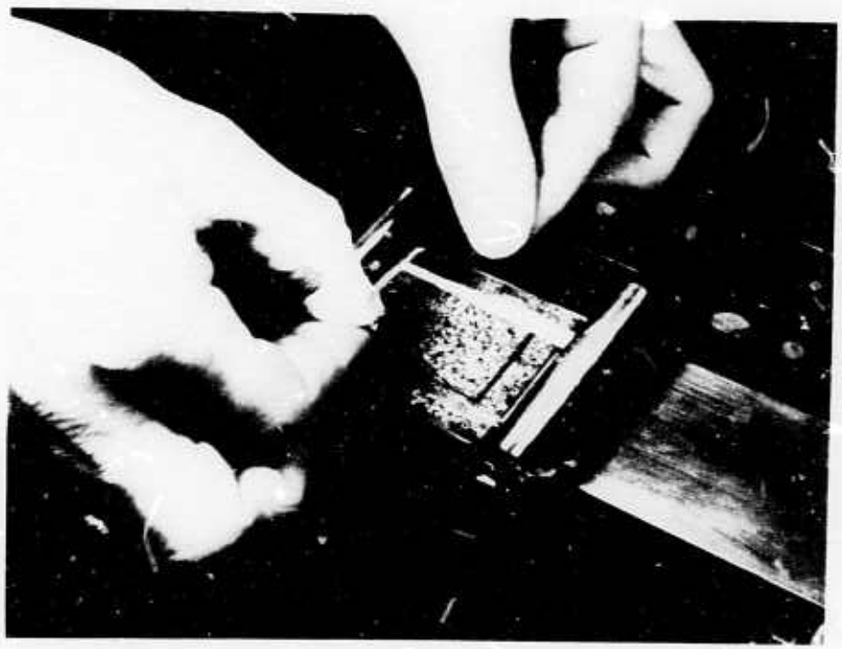

a) Acetate peel being applied to rock slice in third-part compressional loading apparatus.

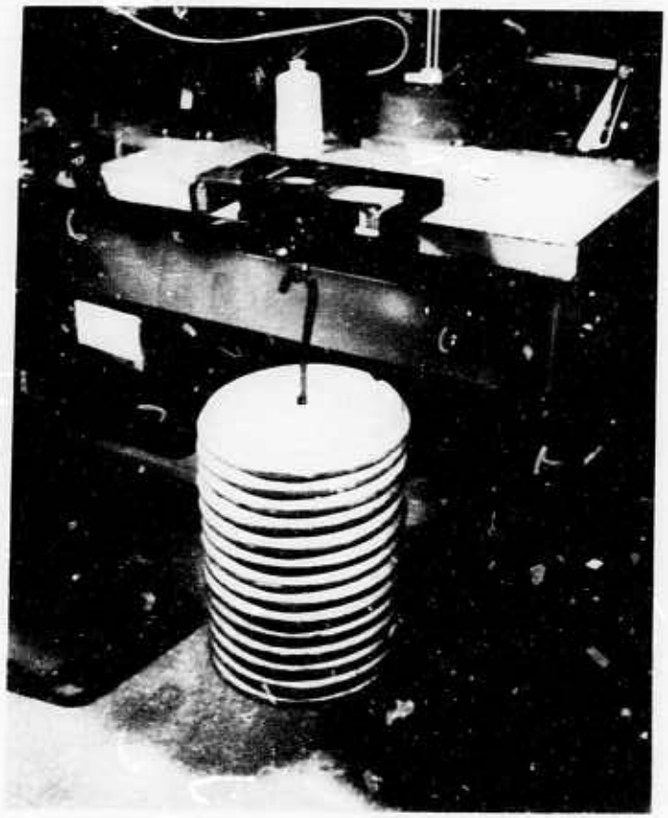

b) Rock slice being tested in third-part compressional loading apparatus. Load of 280 lb (127 Kg) is applied here. Acetate peels are being used to record fabrics in this test.

Figure 6 - Application of acetate peel in third-part compressional loading of rock slide.

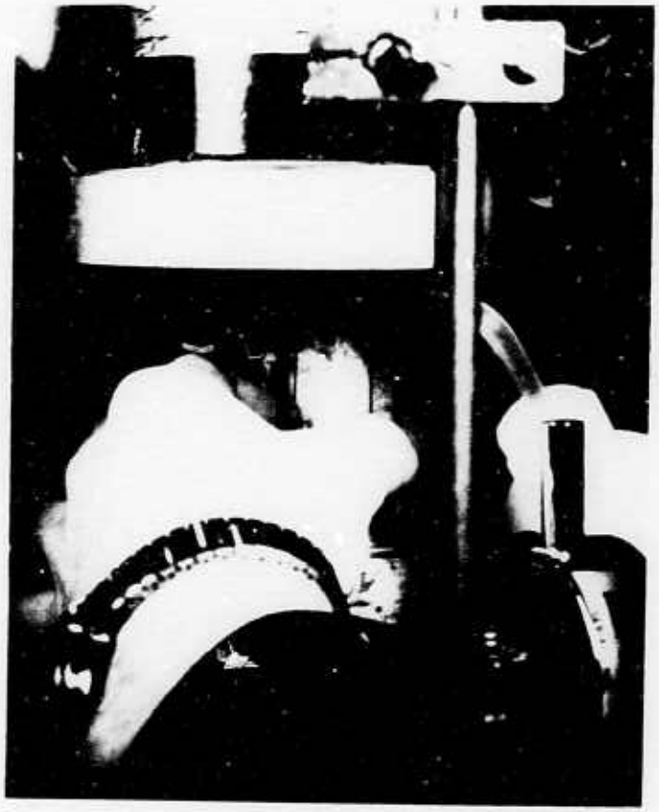

a) Acetate peel being applied to rock cylinder. Peel is held tightly at the bottom while space between peel and rock is filled with acetone from the top.

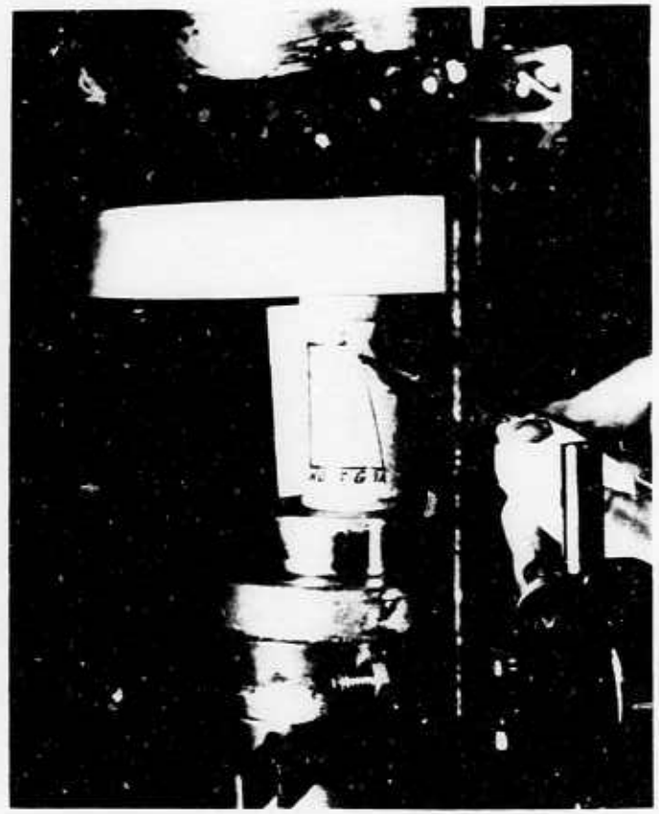

b) Acetate peel being removed from rock cylinder by lifting one side and peeling gently and steadily toward the other side.

Figure 7 - Application and removal of acetate peel in uniaxial compressional testing of rock cylinders.

a) Mounting of acetate peel in 2 in X 2 in (standard 35mm) slide binder. Note identification numbers, registration rectangle, and orientation arrow.

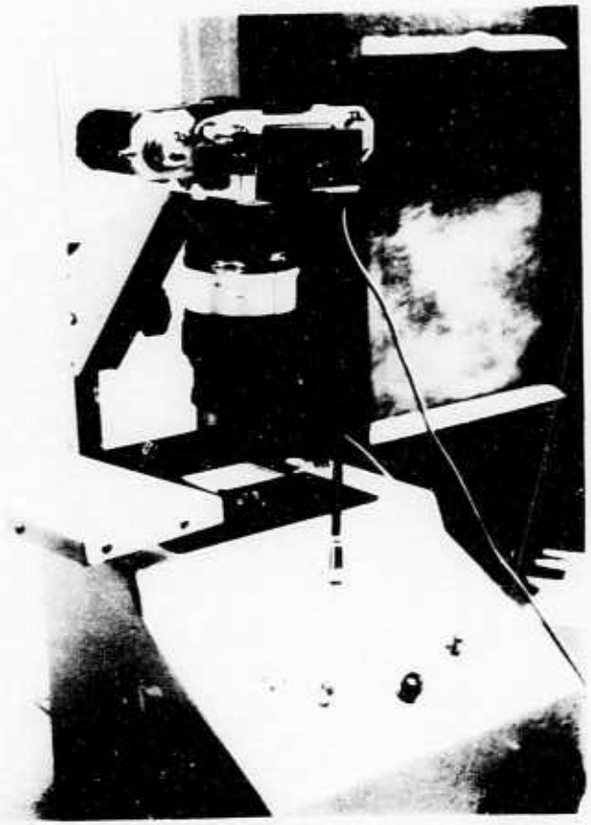

b) Illumitran copy set-up for 35mm. photography of acetate peels to produce input for optical diffraction analysis. Polarizers are placed below peel and below camera lens.

Figure 8 - Mounting and photographic processing of acetate peels.

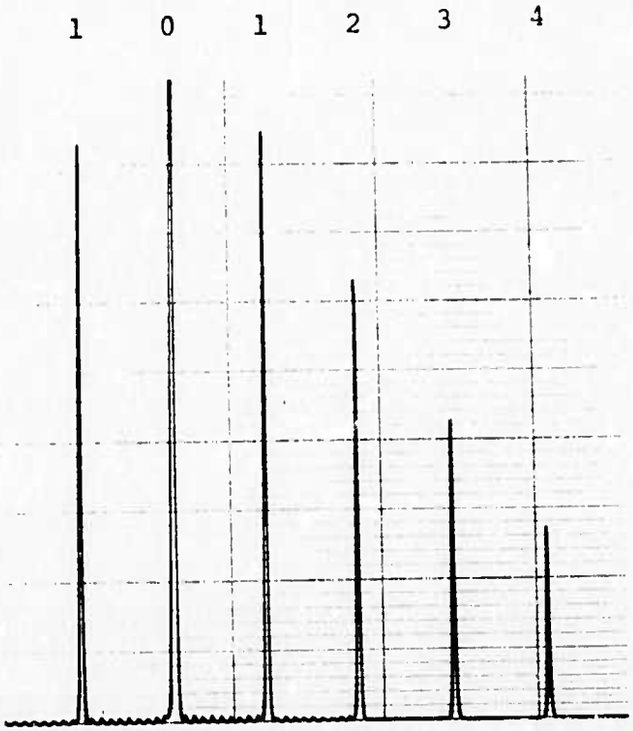

Note approximate symmetry of the two first-order spikes, the approximately linear envelope of the first through fourth spikes, and the nine short spikes between the 0-1, 1-2, and 2-3 spikes. The interval between 0-1, 1-2, 2-3, and 3-4 represents 2.5 lines/mm in the input.

Figure 9 - Profile of calibration transform

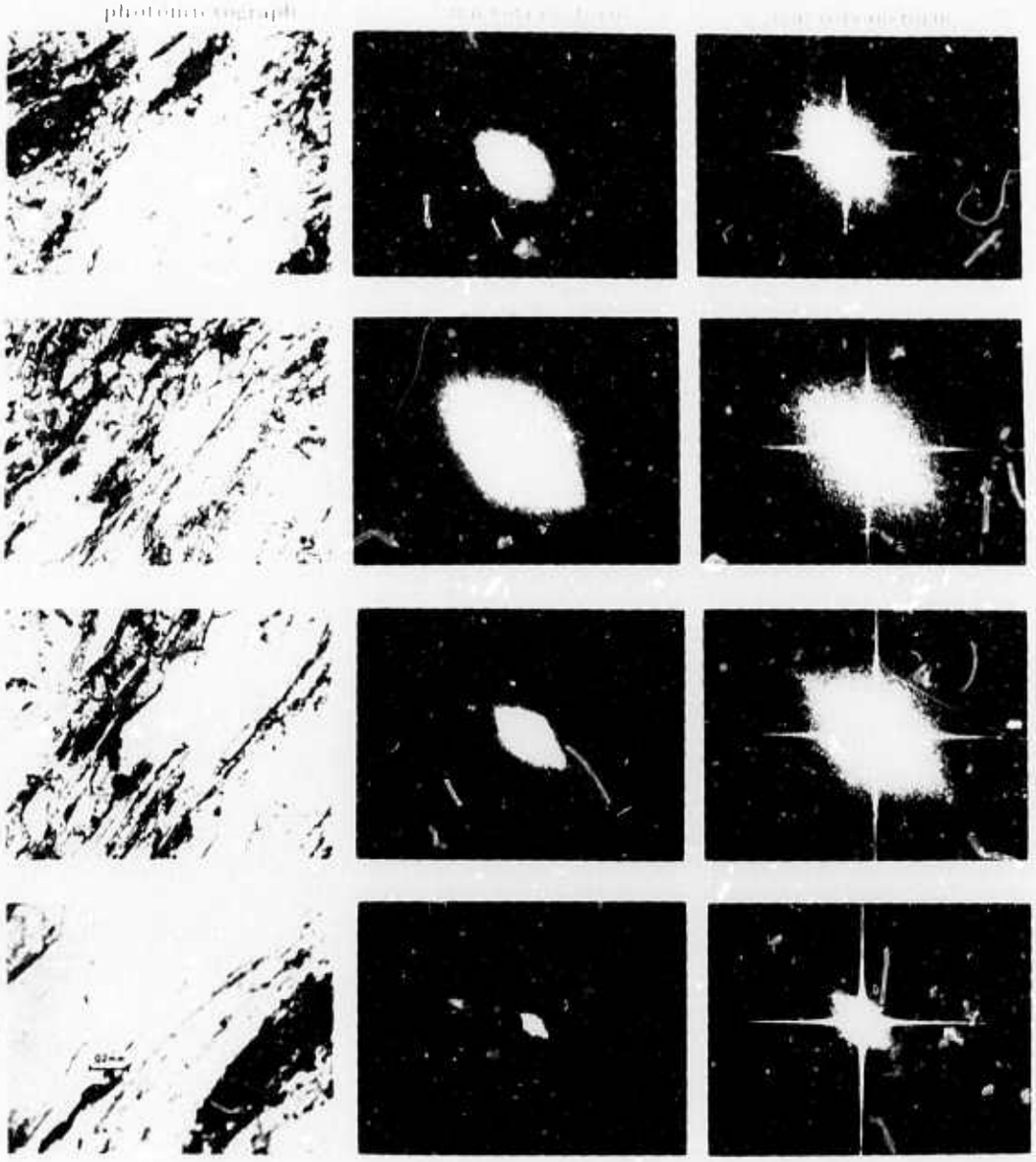

Photomicrograph of a thin-section of a schist with 2.5 X, 6.3X, 16X and 40X objectives (left hand column); their microtransforms (transforms of thin sections via microscope) (center column); and their macrotransforms (transforms of photographs of thin sections via optical bench set-up using Conductron LaserScan C-120 system) (right-hand column). From Power, 1973, Fig. 22.

Figure 10 - Optical processing of thin sections.

Inputs (A-J) and their respective transforms.

A - Vesicular structure in pumice
(Jung, Fig. 123)

B - Granoblastic texture in epidotite.
(Jung, Fig. 95)

C - Quartzose pelite showing a change in sedimentation.
(Jung, Fig. 32)

D - Micaceous pelite
(Jung, Fig. 33)

E - Porphyroblast of oligoclase in a matrix of quartz (predominantly), plagioclase, and biotite.
(Jung, Fig. 85)

F - Fine-grained granulite, crudely layered with lenses of quartz.
(Jung, Fig. 101)

G - Trachyte showing characteristic texture, with some fan-shaped clumps of sanidine.
(Jung, Fig. 142)

H - Phonolite with trachytic structure; sanidine phenocrysts.
(Jung, Fig. 157)

I - Mica gneiss, with quartz and feldspar bands.
(Jung, Fig. 90)

J - Microlitic, porphyritic andesite with plagioclase phenocryst.

Figure 11 - Some reference inputs (line drawings) and their respective transforms.

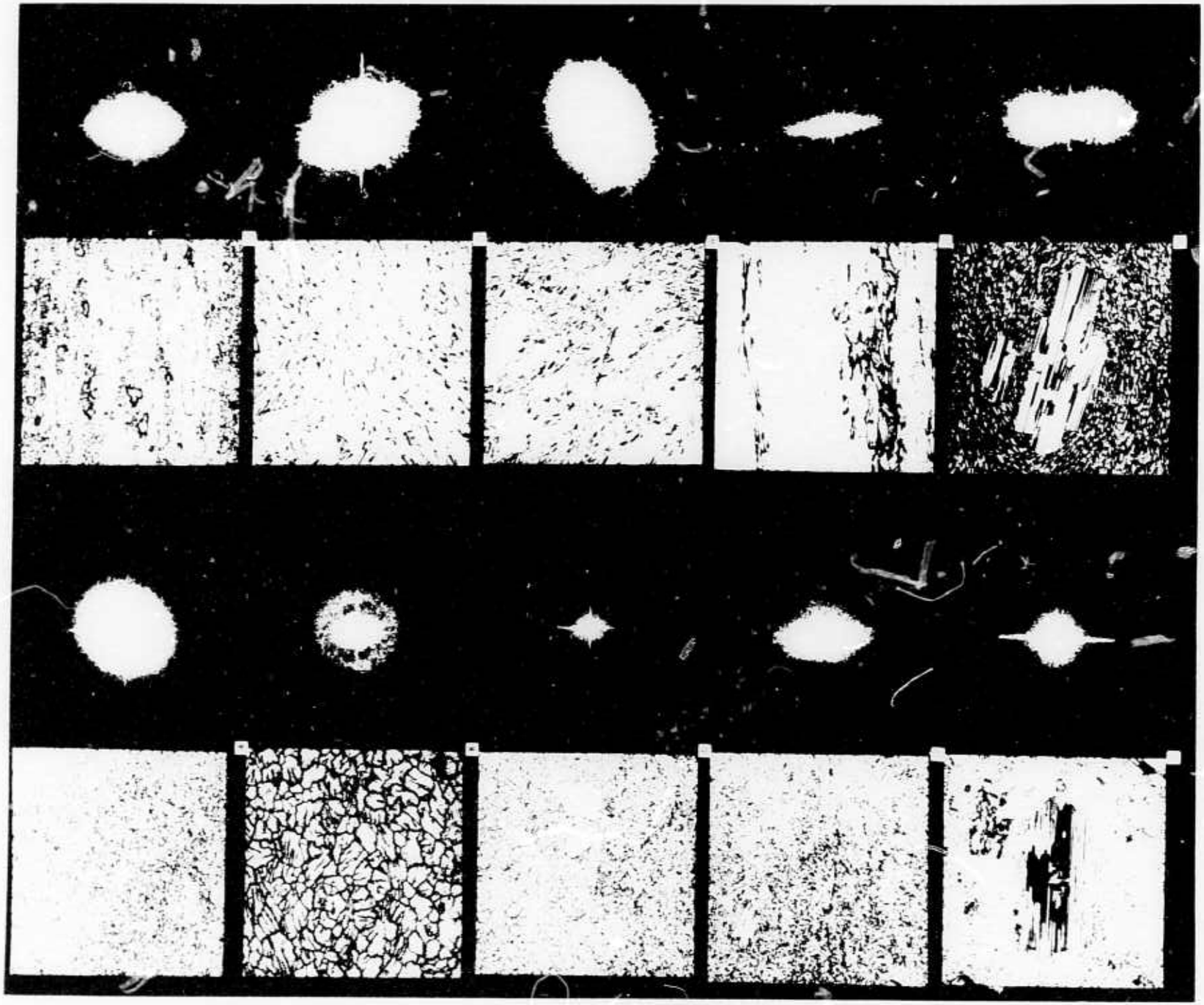

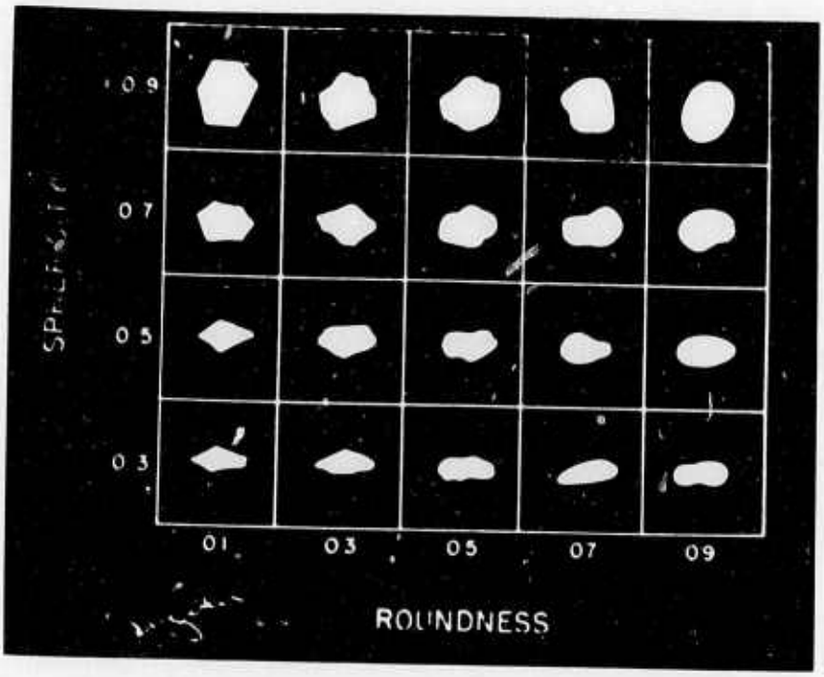

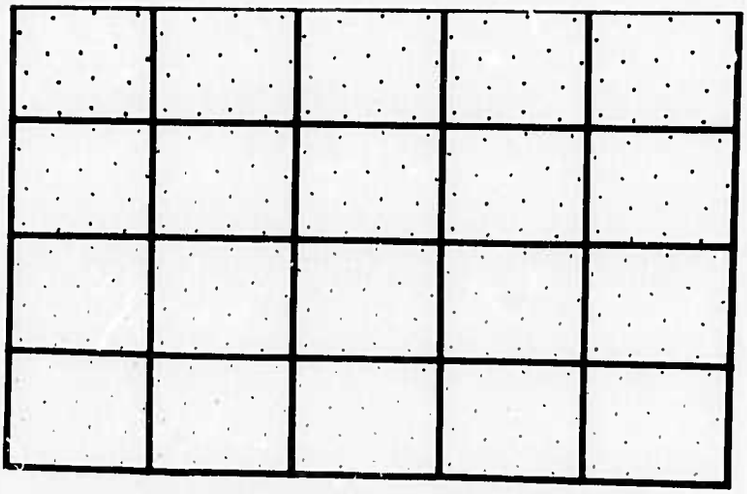

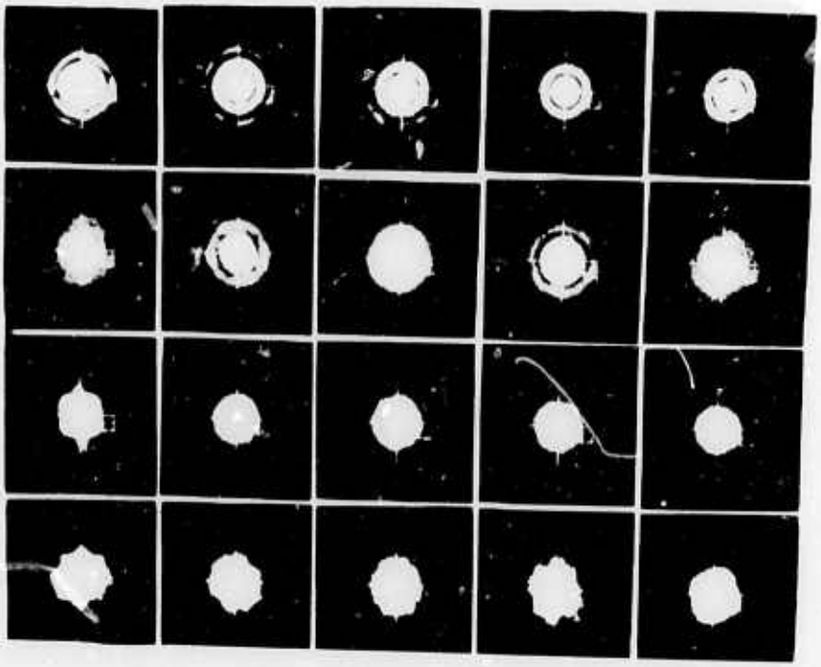

Figure 12 - Idealized particulate shapes and their transforms. (From Larson, 1973, Figures 10, 67, and 68)
a) Sphericity and roundness chart
b) Assemblages of particles such as those in a).
c) Transforms of b).

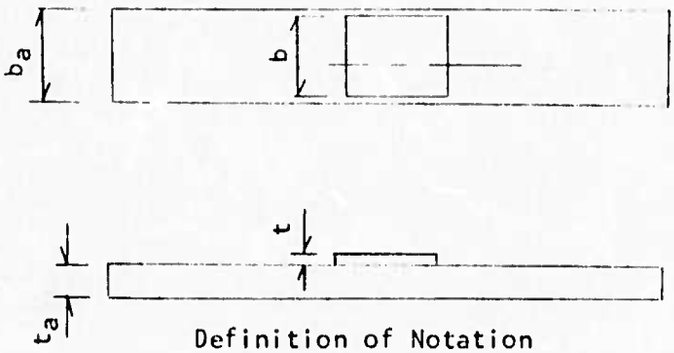

Definition of Notation

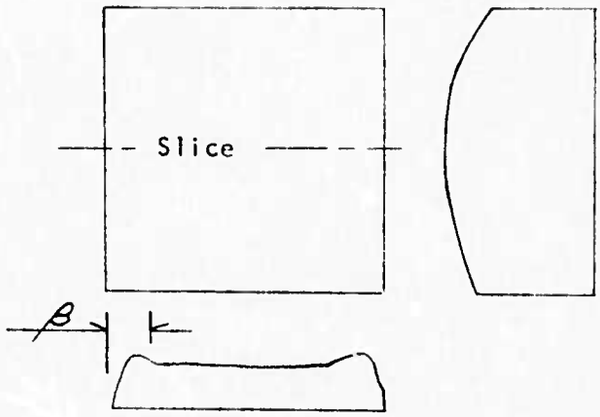

Strain Distributions

a)

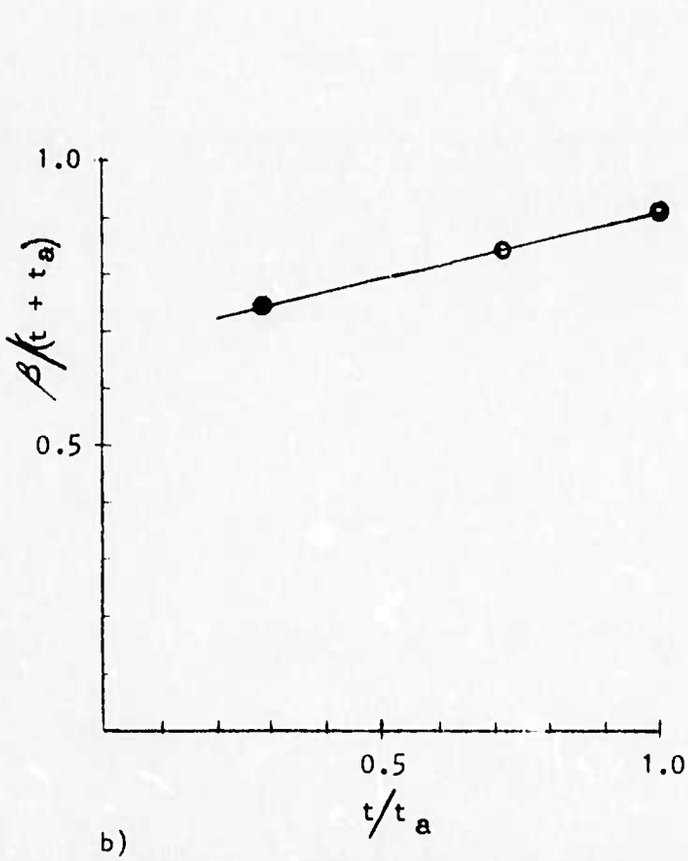

b)

Edge Distance to Uniform Strain

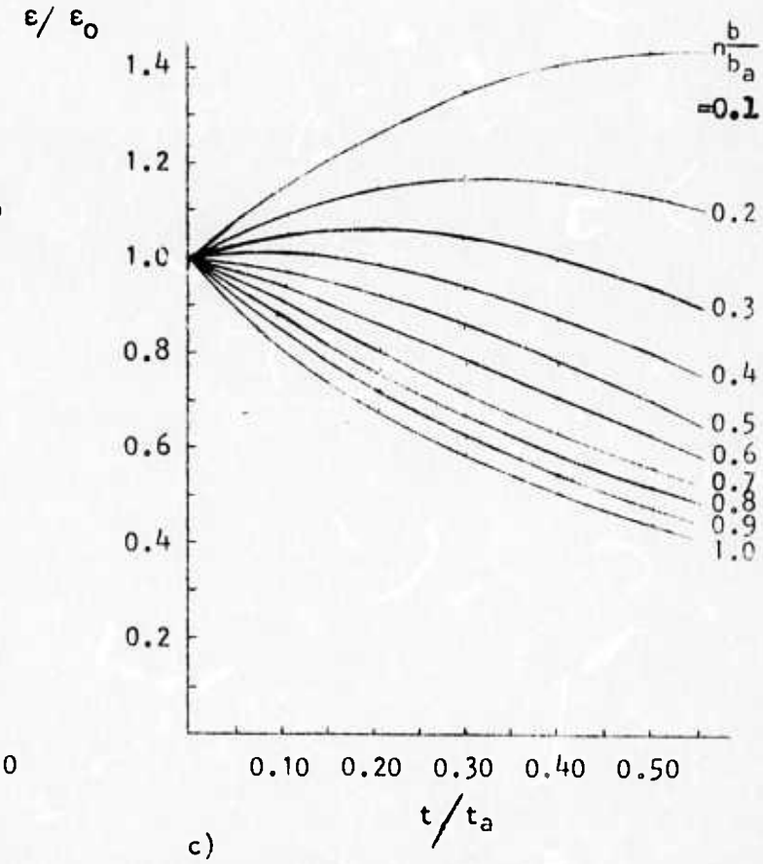

c)

Analytical Strains

Figure 13 - Analysis of Strains in Rock Slices

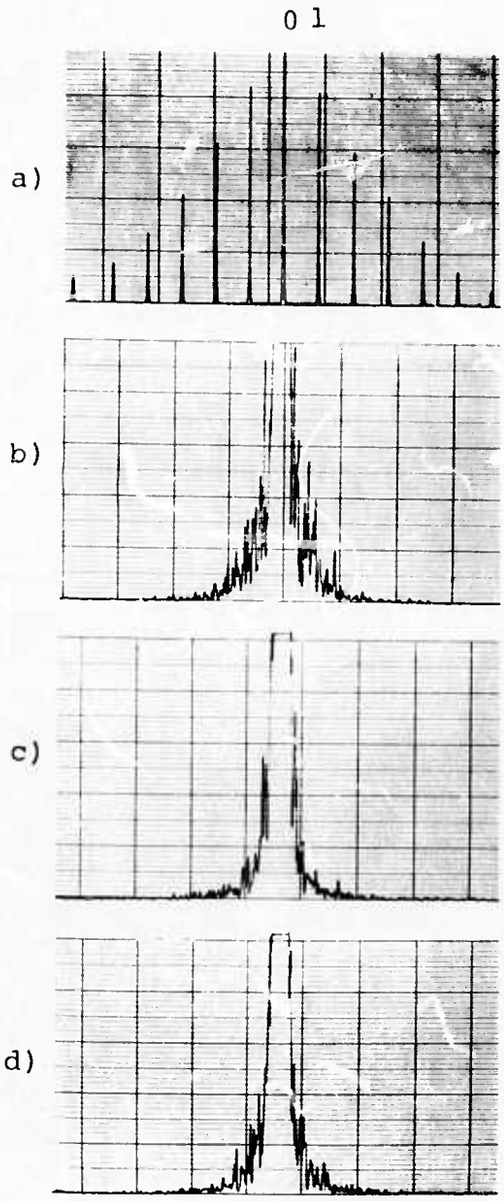

Figure 14 - Profiles of transforms of deformation experiment, uniaxial compression of Tennessee marble cylinder, acetate peel recording.
a) Calibration transform (#4-73/1); 0-1 interval is 2.5 lines/mm
b) No-load transform (#4-73/5); input KO17-Ga-2B
c) Transform (#4-73/8) of loaded specimen; input KO17-Gc-2B. Load 7220 psi (49.78 MN/m^2)
d) Transform (#4-73) of loaded specimen; input KO17-Ge-2B. Load 13540 psi (93.36 MN/m^2)

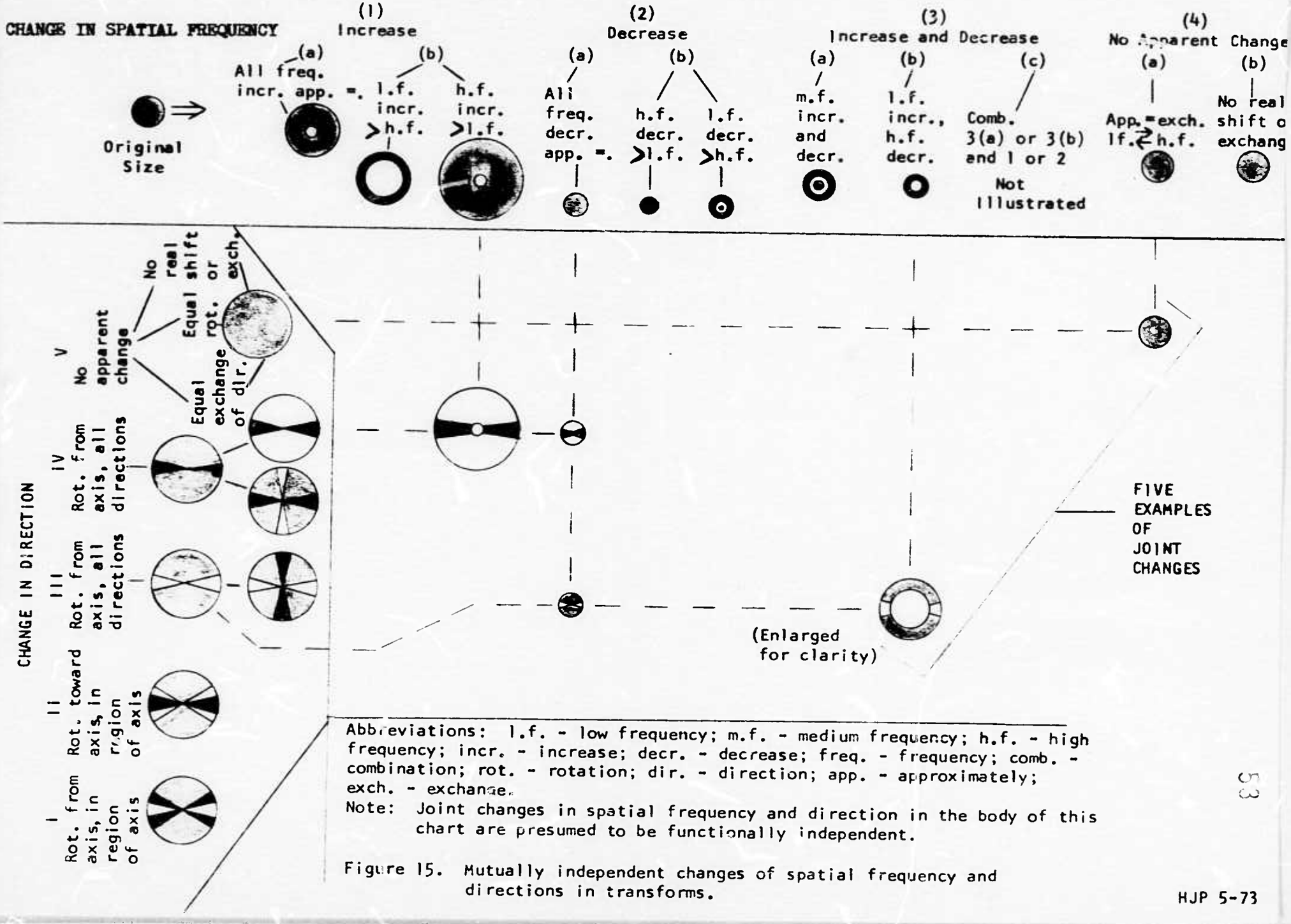

Abbreviations: l.f. - low frequency; m.f. - medium frequency; h.f. - high frequency; incr. - increase; decr. - decrease; freq. - frequency; comb. - combination; rot. - rotation; dir. - direction; app. - approximately; exch. - exchange.

Note: Joint changes in spatial frequency and direction in the body of this chart are presumed to be functionally independent.

Figure 15. Mutually independent changes of spatial frequency and directions in transforms.

HJP 5-73

THREE EXAMPLES OF JOINT, MUTUALLY DEPENDENT CHANGES IN SPATIAL FREQUENCY AND DIRECTION.

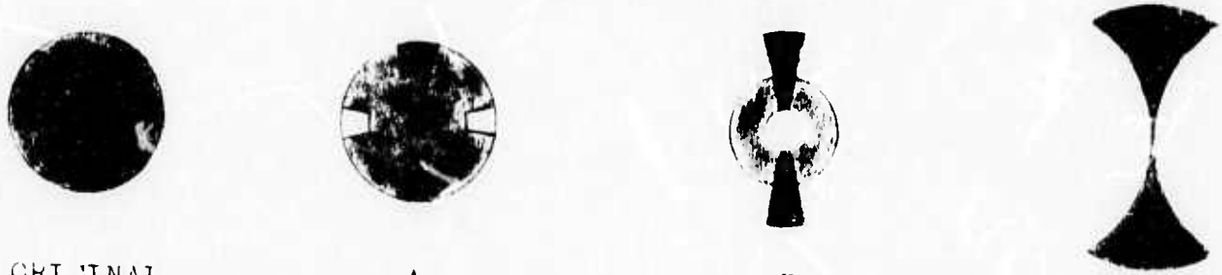

ORIGINAL A B C

A - Rotation toward vertical axis, within high frequency.

B - All low frequency increased and rotated into wedge.

C - Directional spread increases in spatial frequency; net increase in spatial frequency and decrease in direction, with most displacement from low frequency.

Figure 16. Mutually dependent changes of spatial frequency and directions in transforms.

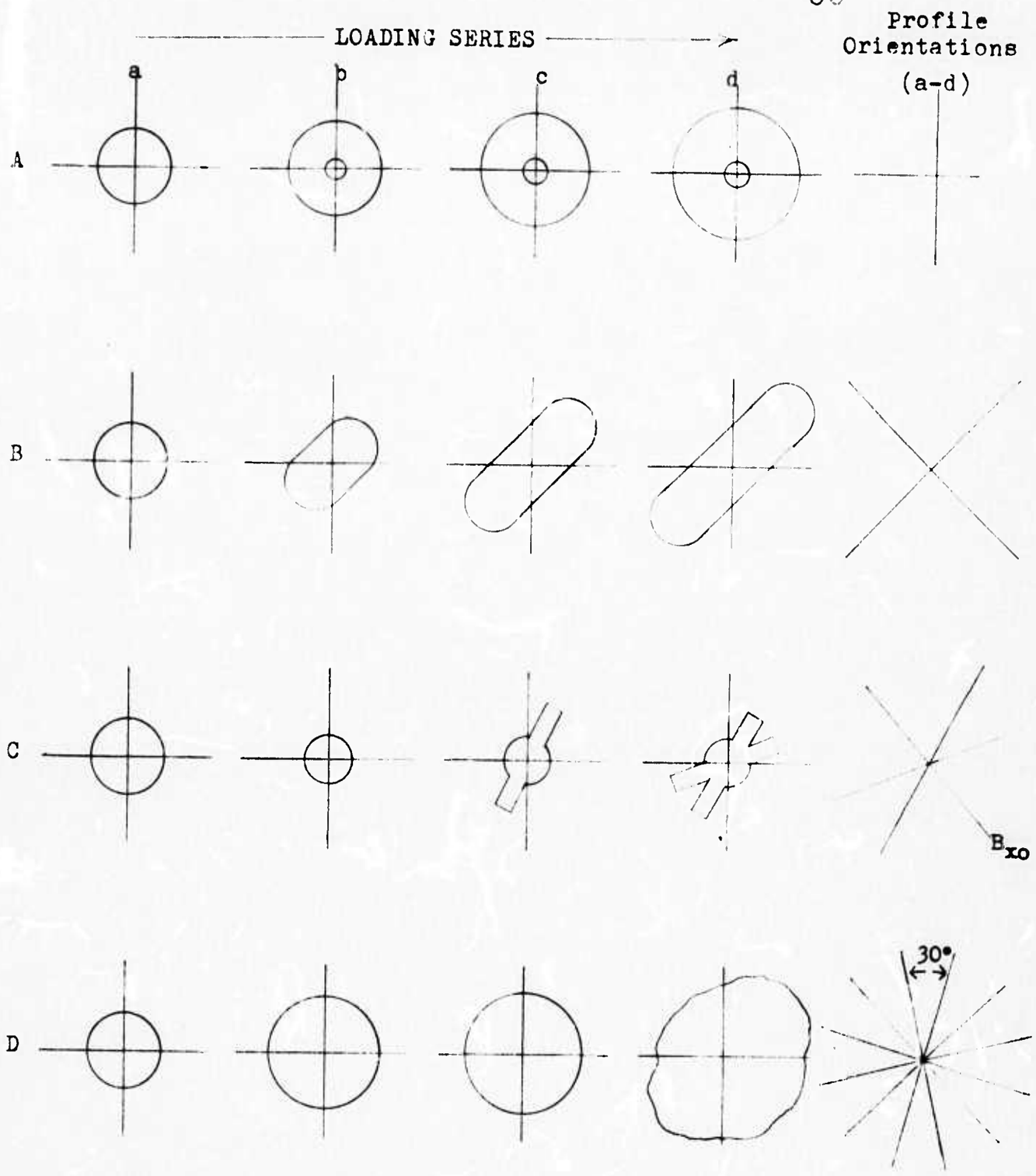

Figure 17. Conventions for profiling transforms. Idealized progressive loading effects are shown in a through d in each row (A-D). Each row (A-D) shows a loading response different from those in the other rows. All rows start with the same transform (column a) for the unloaded state.

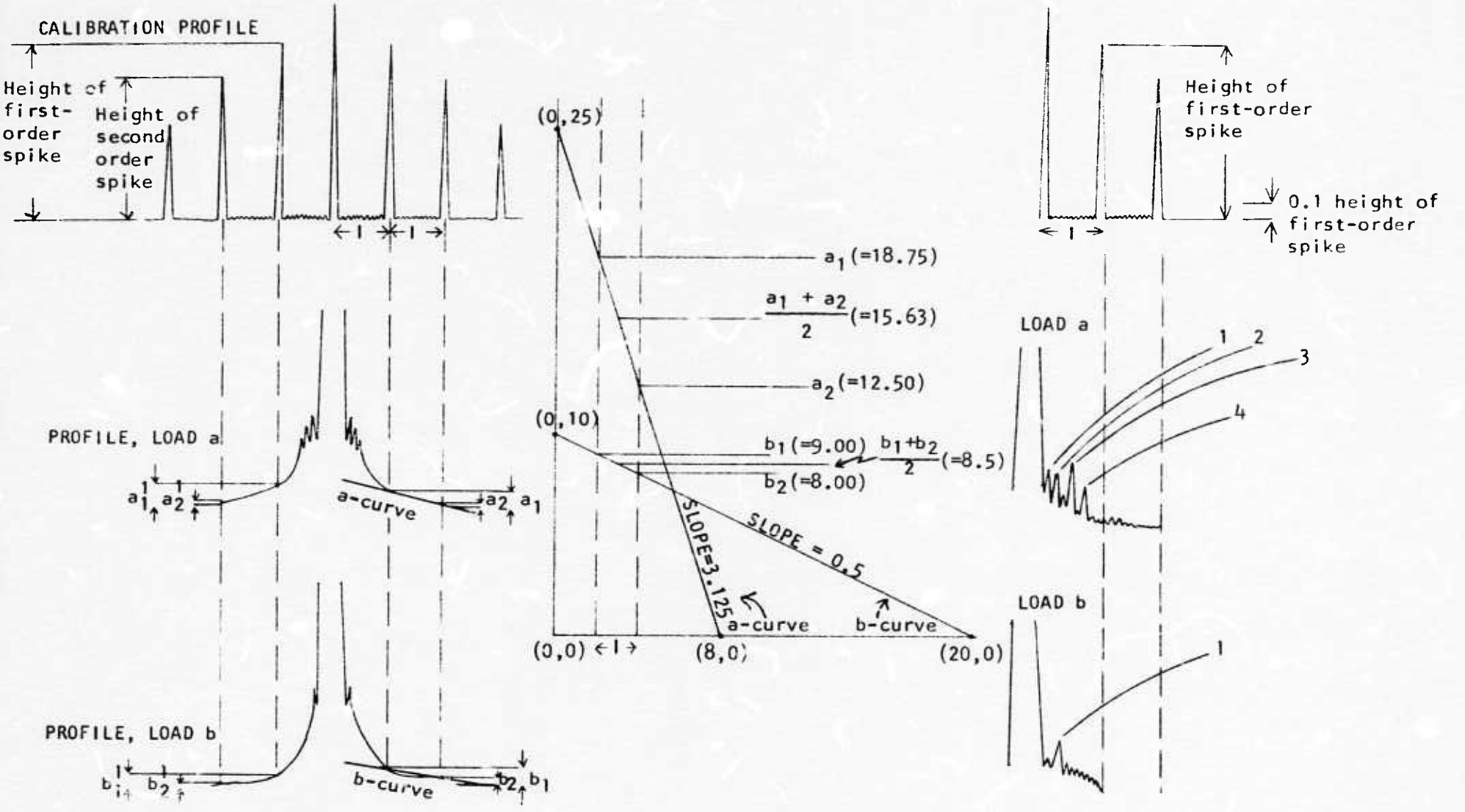

a) Basic Construction

b) Index Based on Change in Spatial Frequency

c) Index of Change in Roughness or Heterogeneity of Profile

Figure 18 - Graphical Analysis of Transform Profiles

APPENDIX B

List of References Consulted

Abbé, Ernst, 1873, Berträge zur Theorie des Mikroskops und der mikroskopischen Wahrenehmung: Archiv für Mikroskopische Anatomie, v. 9, pp. 413-468.

Apostol, T. M., 1964, Mathematical Analysis: Addison-Wesley, Reading, Mass.

Binns, R. A., Dickinson, A. & Watrasiewicz, B. M., 1968, Methods of increasing discrimination in optical filtering: Applied Optics, v. 7, no. 6, pp. 1047-1051.

Born, M. and Wolf, E., 1965, Principles of optics, 3rd Ed.: Pergamon, N. Y., 808 pp.

Bracewell, R. M., 1965, The Fourier transform and its applications: McGraw-Hill, New York, 381 pp.

Bromley, K., Monahan, M. A., Bryant, J. F., and Thompson, B. J., 1971, Holographic subtraction: Applied Optics, v. 10, pp. 171-180.

Cagnet, L. J., 1960, An atlas of optical phenomena: Prentice-Hall, Englewood Cliffs.

Caulfield, H. J., & Lu, S., 1970, The applications of holography: Wiley-Interscience, New York, 138 pp.

Collier, R. J., Barckhardt, C. B., and Lin, L. H., 1971, Optical holography: Academic Press, N. Y., 605 pp.

Cutrona, L. J., Leith, E. N. & Porcello L. J., 1959, Filtering operations using coherent optics: Proc. Nat. Electronics Conference, pp. 262-275.

Cutrona, L. J., Leith, E. N., Palerno, C. J., & Porcello, L. J., 1960, Optical data processing and filtering systems: IRE Trans. Inf. Theory, June, pp. 386-400.

Davis, J. C., 1970, Optical processing of microporous fabrics: in Data Processing in Biology and Geology, J. L. Cutbill, ed., pp. 69-87.

Dobrin, M. B., Ingalls, A. L. and Long, J. A., 1965, Velocity and frequency filtering of seismic data using laser light: Geophysics, v. 30, pp. 1144-1178.

Dobrin, M. B., 1968, Optical processing in the earth sciences: I.E.E.E. Spectrum, Sept. 68, pp. 59-66.

Donath, F. A., Faill, R. T., and Tobin, D. G., 1971, Deformational mode fields in experimentally deformed rock: Geol. Soc. Amer., Bull., v. 82, pp. 1441-1462

Dudderar, T. D., 1969, Applications of holography to fracture mechanics: Soc. for Exper. Stress Anal., Paper No. 1451, 1969 Ann. Mtgs, 13 pp. + 7 Figs.

Esler, J. E., and Preston, F. W., 1967, Fortran IV program for the GE 625 to compute the power spectrum of geological surfaces: Computer Contrib. 16, Kansas State Geol. Surv., 23 pp.

Francon, M., 1963, Modern applications of physical optics: Interscience, New York, 106 pp.

Francon, M., 1966, Diffraction-coherence in optics: Pergamon Press, New York, 137 pp.

Francon, M., 1967, Isotropic and anisotropic media: in Advanced Optical Techniques, ed. by A.C.S. Van Heel, J. Wiley and Sons, N. Y., 678 pp.

Friedman, M., 1969, Petrofabric techniques for the determination of principal stress directions in rocks: Proc., Int. Conf. on State of Stress in the Earth's Crust, Elsevier, pp. 451-552.

Gabor D., Stroke, G. W., Brumm, D., Funkhouser, A., and Labeyrie, A., 1965, Reconstruction of phase objects by holography, Nature, v. 208, no. 5016, pp. 1159-1162.

Gabor D., Stroke, G. W., Restrick, R., Funkhouser, A., and Brumm, D., 1965, Optical image synthesis (complex amplitude addition and subtraction) by holographic Fourier transformation: Physics Letters, v. 18, no. 2, pp. 116-118.

Grebowsky, G. V., 1970, Fourier transform representation of an ideal lens in coherent optical systems: NASA-TR-R-319, Washington, D. C., 62 pp.

Green, A. E., and Adkins, J. E., 1970, Large elastic deformations: Clarendon Press, Oxford, 324 pp.

Gresseth, E. W., 1964, Determination of principal stress directions through an analysis of rock joint and fracture orientations, Star Mine, Burke, Idaho, U. S. Bur. Mines Rept. Inv. 6413, 42 pp.

Gresseth E. W. and Reid, R. R., 1968, A petrofabric study of tectonic and mining-induced deformations in a deep mine: U. S. Bur. Mines Rept. Inv. 7173, 64 pp.

Harbaugh, J. W. and Sackin, M. J., 1967, Fortran IV program for harmonic trend analysis using double Fourier series and regularly gridded data for the GE 625 computer: Computer Contrib. 29, Kansas State Geol. Surv., 30 pp.

Harker, A., 1950 Metamorphism: A study of the transformation of rock masses: 3rd ed., Methuen & Co., 362 pp.

Jackson P. G., 1965, Analysis of variable density seismograms by means of optical diffraction: Geophysics, v. 30, pp. 5-23.

Jaeger, J. C., 1962, Elasticity, fracture, and flow, with engineering and geological applications: 2nd Ed., Wiley, 152 pp.

Jaeger, J. C. and Cook N. G. W., 1969, Fundamentals of rock mechanics: Methuen, London, 513 pp.

James, W. R., 1966, The Fourier series model in map analysis: Tech. Rept. No. 1, ONR Task No. 388-078, Contract Nonr-1228(36), Geography Branch, O.N.R., 37 pp.

Jenkins, R. W., 1969, Holographic optical data processing: NASA Tech. Memo. Rept. No. 53961, N70-17359, Marshall Space Flt. Ctr., Ala., 26 pp.

Jennison, R. C., 1961, Fourier transforms and convolutions for the experimentalist: Pergamon Press, New York, 120 pp.

Judd, W., 1969, Statistical methods to compile and correlate rock properties and preliminary results: ARPA Contract DACA 73-68-C-0002(P0002) Tech. Rept. No. 2, 109 pp.

Jung, J., 1969, Precis de Petrographie: Roches sedimentaires, metamorphiques et eruptives: 3rd Ed., Masson, 332 pp.

Kingslake, R., ed., 1967, Applied Optics and optical engineering: Academic Press, New York, vols. 1-5.

Krumbein, W. W., 1966, A comparison of polynomial and Fourier models in map analysis: Tech. Rept. No. 2, ONR Task No. 388-078, Contract Nonr-1228(36), Geography Branch, O.N.R., 45 pp.

Larson, W. C., 1972, A study of particle parameters to determine the fragmentation history of test rock and mineral samples: M. S. Thesis, Univ. of Wis.-Milw., 195 pp.

Levi, L., 1968, Applied optics: John Wiley and Sons, New York.

Levy, M., 1967, Wide latitude photography: Phot. Sci. Eng., v. 11, no. 1, pp. 46-53.

Lipson, S. G. and Lipson, H., 1969, Optical physics: Cambridge Univ. Press, Cambridge, 494 pp.

Lurie M., 1968, Fourier-transform holograms with partially coherent light: holographic measurement of spatial coherence: Jour. Opt. Soc. Amer., v. 58, no. 5, pp. 614-628.

Markham, R., Frey, S., and Hills, G. J., 1963, Methods for the enhancement of image detail and accentuation of structure in electron microscopy: Virology, v. 20, pp. 88-102.

Markham, R., Hitchborn, J. H., Hills, G. J., and Fred. S., 1964, The anatomy of the tobacco mosaic virus: Virology, v. 22, pp. 342-359.

Mitchel, R. H., 1969, Application of optical data processing techniques to geological imagery: Clearinghouse for Federal Scientific and Technical Information, Springfield, AD 695 120, 35 pp.

O'Neill, E. L., 1963, Introduction to statistical optics: Addison-Wesley, Reading, Mass., 179 pp.

Obert, L. A., and Duvall, W. I., 1967, Rock mechanics and the design of structures in rock: Wiley, 650 pp.

Orhaug, J. and Svenssen, H., 1971, Optical processing for pattern properties: Photogrammetric Engrg., pp. 547-554.

Parrent, G. B., Jr. and Thompson, B. J., 1969, Physical optics notebook: Soc. of Photo-optical Inst. Eng., Redondo Beach, Cal., 63 pp.

Pennington, K. S. and Harper, J. S., 1970, Techniques for producing low-noise, improved efficiency holograms: Applied Optics, v. 9, pp. 1643-1650.

Peterson, R. A., and Dobrin, M. B. (Eds.), 1966, A pictorial digital atlas: United Geophysical Corp., Pasadena, 53 pp.

Pincus, H. J., 1966, Optical data processing of vectorial rock fabric data: Proc. First Int. Cong. on Rock Mechanics, v. 1, pp. 173-177.

Pincus, H. J. and Dobrin, M. G., 1966, Optical processing of geological data: Jour. Geophys. Res., v. 71, no. 20, pp. 4861-4870.

Pincus, H. J. and Ali, S., 1968, Optical data processing of multispectral photographs of sedimentary structures: Journal of Sedimentary Petrology, v. 38, no. 2, pp. 457-461.

Pincus, H. J. and Gardner, R. D., 1968, Fluorescent dye penetrants applied to rock fractures: Int. J. Rock Mech. and Min. Sci., v. 5, no. 2, pp. 155-158.

Pincus, H. J., 1969a, Sensitivity of optical data processing to changes in fabric-Part I-geometric patterns; Part II-standardized grain size patterns; Part III-rock fabrics: Int. Jour. Rock Mech. Min. Sci., v. 6, pp. 259-276.

Pincus, H. J., 1969b, The analysis of remote sensing displays by optical diffraction: Proc., 6th Int. Symp. on Remote Sensing of Environment, U. Mich., v. 1, pp. 261-274.

Pincus, H. J., 1970, The analysis of two-dimensional displays by optical diffraction with examples from the earth sciences: Proc., Electro-Optical Systems Design Conf., 1969, Industrial and Sci. Conf. Mgmt., pp. 625-632.

Pincus H. J., Power, P. C., Jr., and Woodzick, T. (In press) Analysis of contour maps by optical diffraction: GEOFORUM, Wolfsburg, Germany.

Power, P. C., 1973, Optical diffraction analysis of petrographic thin sections: M. S. Thesis, Univ. Wis.-Milw., 193 pp.

Preston, F. W. and Harbaugh, J. W., 1965, BALGOL programs and geologic application for single and double Fourier series using IBM 7090/7094 computers: Spec. Dist. Pub. 24, Kansas State Geol. Surv., 72 pp.

Preston, F. W. and Davis, J. C., 1972, Application of optical processes to geological images: Symp. vol.13,Inst. of Physics, London, Machine perception of patterns and pictures, Teddington Conf., pp 223-232.

Ramsey, J. G., 1967, Folding and fracturing of rocks: McGraw-Hill, New York, 568 pp.

Robinson, J. E., Charlesworth, H.A.D., and Kanasewich, E. R., 1968, Spatial filtering of structural contour maps: XXIII International Geol. Cong., v. 13, pp. 163-173.

Rosenfeld, Azriel, 1969, Picture processing by computer: Academic Press, New York, 196 pp.

Rosten, P., 1967, Image spectrum analyzer: A. F. Syst. Comm., Aerospace Rept. No. TR-1001 (2307)-17, A. F. Report No. SSD-TR-67-160, AD 662718, Los Angeles, 12 pp. + App. A-D.

Sander, B., 1970, An introduction to the study of fabrics of geological bodies: Transl. by F. C. Phillips and G. Windsor, Pergamon, New York, 641 pp.

Sherr, S., 1970, Fundamentals of display system design: Wiley-Interscience, New York, 484 pp.

Shulman, A. R., 1970, Optical data processing: John Wiley & Sons, New York, 710 pp.

Smith, H. M., 1969, Principles of holography: Wiley-Interscience, New York, 239 pp.

Sommerfeld, Arnold, 1954, Lectures on theoretical physics, v. IV-Optics: Academic Press, New York, 383 pp.

Steckley, R. C., 1972, Determination of paleotectonic principal stress direction, including analysis of joints by optical diffraction, U. S. Bur. Mines, Rept. Inv. 7706, 18 pp.

Stroke, G. W., 1966, An introduction to coherent optics and holography: Academic Press, New York, 358 pp.

Tetelman, A. S. and McEvily, A. J., Jr., 1967, Fracture of structural materials: J. Wiley, New York, 697 pp.

Tobin, D. G. and Donath, F. A., 1971, Microscopic criteria for defining deformational modes in rock: Geol. Soc. Amer., Bull., v. 82, pp. 1463-1476.

Turner, F. J. and Weiss, L. E., 1963, Structural analysis of metamorphic tectonites: McGraw-Hill, New York, 545 pp.

Vanderlugt, A., 1964, Signal detection by complex spatial filtering: IEEE Trans. Inf. Theory, IT-10, pp. 139-145.

Vanderlugt, A., 1966, Practical considerations for the use of spatial carrier-frequency filters: App. Opt., v. 5, pp. 1760-1765.

Vistelius, A. B., 1966, Structural diagrams: Transl. by R. Baker, transl. edited by N. L. Johnson and F. C. Phillips, Pergamon, New York, 178 pp.

Wahlstrom, E. E., 1969, Optical crystallography: John Wiley & Sons, New York.

Webb, R. H., 1969, Elementary wave optics: Academic Press, New York, 268 pp.

Weinberger and Almi, 1971, Interference method for pattern comparison: Applied Optics, v. 10, pp. 2482-2487.

Whitten, E. H. J., 1966, Structural geology of folded rocks: Rand McNally, Chicago, 663 pp.

Willard, R. J. and McWilliams, J. R., 1969, Microstructural techniques in the study of physical properties of rock: Int. J. Rock Mech. Min. Sci., v. 6, pp. 1-12.

Yu, F. T. S. and Bieringer, R. J., 1971, Optical correlation analysis of two-phase micrographs: Applied Optics, v. 10, p. 2269.

Appendix C

New or Modified Procedures and Lists

1. Procedure for preparation of test samples
2. Data sheet for specimens in rock slice tests
3. Test identification code numbers for cylinder uniaxial loading experiments
4. Test identification code numbers for cantilever and three-part loading experiments
5. Acetate peel and photograph identification numbers
6. Data sheet for loading experiments
7. Acetate sheet peel technique for rock cylinders
8. Some characteristics of film used in this project
9. Darkroom procedures
10. Procedure for mapping transforms
11. List of available photographic equipment
12. Scale conversion in inputs and transforms

Note: Procedures and lists appearing in earlier semiannual and annual reports and in which there have been no subsequent changes are not reproduced here.

Procedure for Preparation of Test Samples

I Preparation of slices

a) A 2 X 12 X 12 in. (50.8 X 304.8 X 304.8 mm) slice was sawed at a local quarry from a one-foot (304.8 mm) cube of each of the eight ARPA rocks.

b) From the 2 X 12 X 12 in. (50.8 X 304.8 X 304.8 mm) slabs 2 prisms were cut, the first 2 X 2 X 12 in. (50.8 X 50.8 X 304.8 mm) and the second 2 X 2 X 10 in. (50.8 X 50.8 X 254 mm).

c) The prisms were then locked into a Hillquist 20 in. (508 mm) saw and serial slices were sawed which ranged in thickness from .075 in. (1.91 mm) to .110 in. (2.80 mm)

d) Each slice was then ground on a lap wheel using 120 grit to a thickness of .070 in. (1.78 mm) to .090 in. (2.29 mm)

e) The slices were then final-lapped using 400 grit to a thickness which ranged from .065 to .085 in. (1.65 to 2.16 mm) with a variation in flatness not greater than $\pm$ .002 in (.051 mm)

f) The slice was then glued to an aluminum bar using Hysol Epoxi-Patch

g) A uniform and constant glue thickness was maintained during the setting process by using a small 20 lbs. (89N) spring clamp to apply stress and a metal plate between rock and clamp to distribute the stress. Glue thickness is approximately .003 in. (.076 mm)

II Preparation of Prisms

a) Same as a and b above

b) Samples were sawed on Hillquist 20 in. (508 mm) saw to $\approx$ 4.5 cm X 1.5 cm X 2.5 cm

c) Samples were finished on Brown and Sharp No. 2 surface grinder to the final dimensions of 4 cm X 1 cm X 2 cm

III Preparation of cylinders

a) Cores were sawed to a length that was slightly greater than 2 1/4 times the width

b) Core ends were then ground on a Brown and Sharp No. 2 surface grinder to a length to width ratio between 2:1 and 2 1/4 : 1

Data sheet for specimens in rock slice tests.

Test Identification No._____

Rock Slice No._____

Rock Type _____

Acetate Peel ____ Regular Photography ____

Fluorescent Dye Photography ____

Operator _____ Date _____

Strain Gage Data

Resistance
Gage Factor: Rock_____ Bar_____
F_{box}

Specimen Dimensions and Orientation and Gage Location

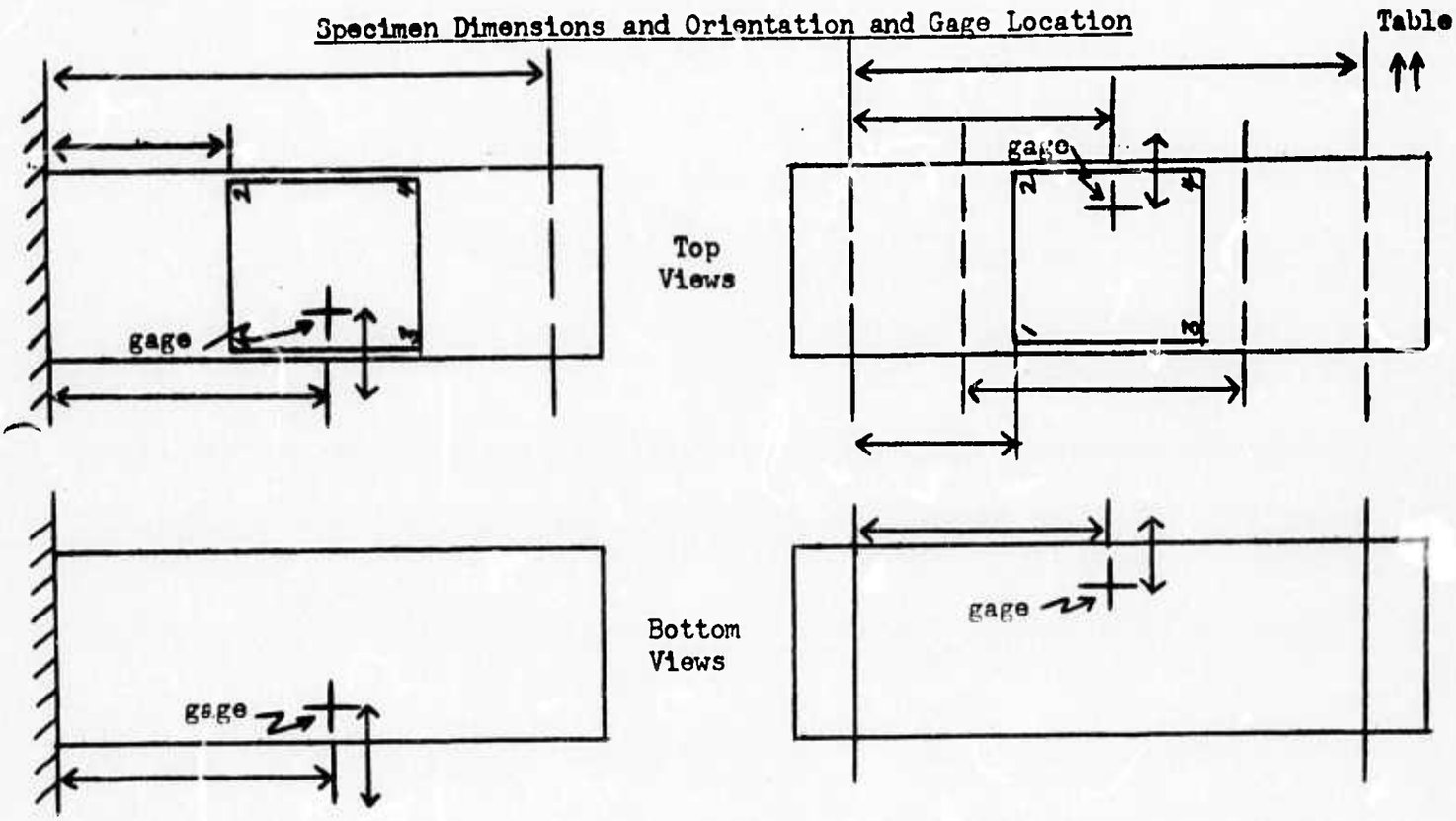

Cantilever Loading Apparatus

Three-Part Loading Apparatus

Comments:

Rock Slice Thickness Data (inches)

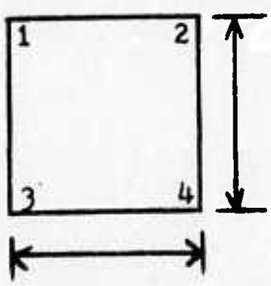

Al Bar Thickness 0.25
Slice Thickness_____
Corner Thickness:
1 2 3 4

Rock + Al Bar + Epoxy

Epoxy

TEST IDENTIFICATION CODE NUMBERS FOR CYLINDER UNIAXIAL LOADING EXPERIMENTS

First Digit - capital letter indicating type of test
K = cylinder, uniaxially loading

Second Digit, Third Digit, Fourth Digit } numerals indicating the number of the test

Fifth Digit - capital letter indicating general rock type
A = acid igneous
B = basic igneous
I = intermediate igneous
S = sandstone
L = limestone
D = dolomite
M = shale, mudstone
C = conglomerate
F = foliated or lineated metamorphic
G = nondirectional structure metamorphic

Sixth Digit - a numeral indicating the face of the rock slab from which the test specimen was cut

Seventh Digit - a letter indicating the position of the cylinder with respect to the original core length from which it was cut. See diagram below.

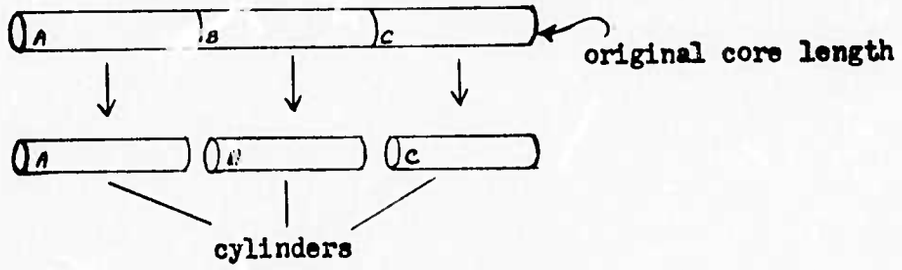

For photographic registration purposes, a rectangle 24 x 35 mm is used. An arrow indicates the "top" position during loading.

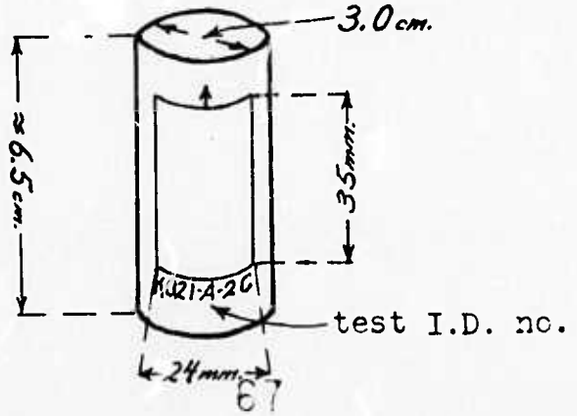

TEST IDENTIFICATION CODE NUMBERS FOR CANTILEVER & THREE-PART LOADING EXPERIMENTS

First Character - capital letter indicating type of test
- C = cantilever weight loaded
- M = cantilever micrometer loaded
- P = three-part loading

Second Character, Third Character, Fourth Character } numerals indicating the number of the test

Fifth Character - capital letter indicating general rock type
- A = acid igneous
- B = basic igneous
- I = intermediate igneous
- S = sandstone
- L = limestone
- D = dolomite
- M = shale, mudstone
- G = conglomerate
- C = chemical (evaporite, chert, etc.)
- O = organic (coal)
- F = foliated or lineated metamorphic
- N = nondirectional structure metamorphic

Sixth Character - a numeral indicating the face of the rock slab from which the test specimen was cut

Seventh Character - a capital letter indicating whether the test was compressional or tensional
- C = rock slice tested in compression
- T = rock slice tested in tension

An example of the above code number for a cantilever loaded, compressional test on an acid igneous rock cut from face one of the rock slab would be the following:

C001-A-1C

This is the test identification number that appears in the upper right hand corner of each data sheet corresponding to that particular test.

ACETATE PEEL & PHOTOGRAPH IDENTIFICATION NUMBERS

Acetate peels and photographs corresponding to specific loads are identified by the small letter which appears in the far left hand column of the second page of the data sheets for each test. (Column headed "Peel ID No." or "Photo ID No.")

Each photograph and acetate peel is individually coded with its complete corresponding test identification number, plus the small letter which identifies that particular photograph or peel. This small letter is inserted after the fifth digit of the test identification number.

An example of an identification number on a photograph or peel whose corresponding test identification number is C001-A-1T would be the following:

C001-Aa-1T

On cantilever and three-part loading tests, rectangles are used to aid photographic comparison.

On cantilever weight loaded and cantilever micrometer loaded, a rectangle open at one end is used; the open end of the rectangle points in the direction of the applied load.

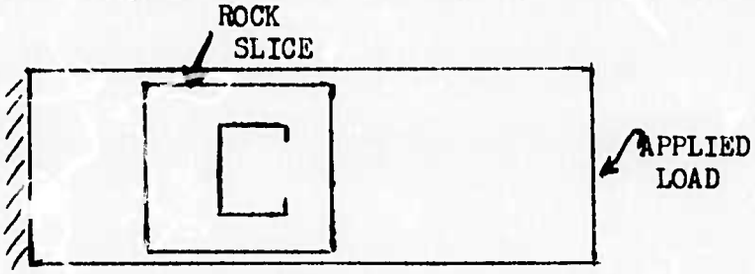

On three-part loading tests, a rectangle whose length parallels the width of the bar is used.

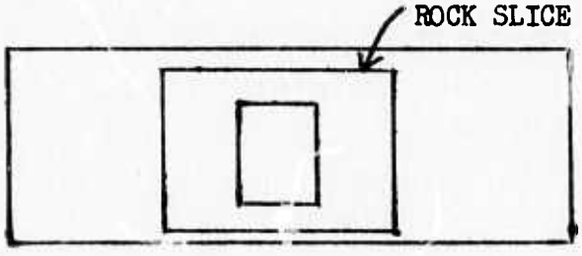

Data sheet for loading experiments.

Test Identification No. ____________

Operator ____________ Date ____________

Peel or Photo ID Letter	Increment Load or Micrometer Reading	Total Load or Total Deflection	Gage ______ Channel No.		Gage ______ Channel No.			
			Indicator Reading	Exp. Strain	Indicator Reading	Exp. Strain		

Acetate sheet peel technique for rock cylinders.

Materials: a. Acetone
b. 3 mil clear acetate sheets

1. Clean rock cylinder registration area by application of 2-6 acetate peels. (Depending on rock type.)

2. Ink specimen with registration rectangle, top arrow, and test identification number.

3. Cut acetate sheet at least ⅛ inch larger than registration rectangle, but leaving it short enough to allow placement of acetone bottle nozzle above peel on specimen surface when in test position.

4. With rock core in place, bend acetate peel around core, holding it tight about its partial circumference at the bottom, but keeping an eighth-inch gap between peel and rock at the top.

5. With other hand inject acetone at the top into the space between peel and rock letting it fill that space for the briefest possible time.

6. Quickly slide fingers up from bottom of peel, pulling entire peel surface into contact with rock causing excess acetone to squirt out at the top.

7. Allow to dry for 5 minutes.

8. Remove peel from surface with a slow gentle peeling motion from one side of the surface to the other side.

9. Place peel between flat surfaces and apply pressure to prevent curling of the peel for about one hour.

10. Slides are made of peels by placing them between glass plates and sealing the edges.

Some characteristics of film used in this project

Film	Size	ASA	Inputs	Outputs	Remarks
Panatomic X	35mm	32	Good contrast Good resolution; Fine grain; Best film for normal contrast subjects	Good contrast Good resolution; Fine grain; Currently used for all transform	Used in most of of our applications as inputs and outputs
Panatomic X	120	32	Same as above	Too large format for continuing use	Most commonly used film and format holographing specimens under load in rock mechanics experiments.
Plus X	35mm	125	Good contrast; Good resolution; moderate grain	Good contrast; Good resolution; moderate grain	More grainly than Pan X, therefore not used.
Tri X	35mm	400	Continuous tone inputs; grainy	Microtransforms; grainy	Useful where light levels are low, as in microscopy.
SO 410	35mm	160	Not tried	high red sensitivity; good grain, resolution and speed	New Kodak film - may be very useful in future applications.
Kodalith	35mm 4X5 in.	6	Good for line drawings (binary inputs)	not red sensitive; binary spatial filters	Pinholes are caused in developing; must be retouched

Film	Size	ASA	Inputs	Outputs	Remarks
High Contrast Copy	35mm	25	Good for line drawings (binary inputs)	too much contrast	Difficult to determine proper ASA. Thin base leads to problems in gate.
Agfa Geveart 10E75	35mm 2X3 in. plates	?	Very high resolution; very high contrast	Slow; poor transforms; good for holography	Difficult to determine proper exposure
Polaroid 55 p/n	4X5 in.	50			Good for spot checks
Polaroid 57	4X5 in.	3000			Good for spot checks; very fast.

Darkroom Procedures:

FILM	ASA	DEVELOPER	TEMP.	MIXTURE	TIME
PANATOMIC x/35mm	32	D76	68°f	1:1	8 1/2 min.
PANATOMIC x/120	32	D76	68°f	1:1	10 min.
Plus X /35mm	125	D76	68°f	1:1	9 min.
Tri X /35mm	400	D76	68°f	1:1	10 min.
Tri X /35mm	1200	Acutine	75°f	stock	3 3/4 min.
Kodalith /4X5"	6	Kodalith A+B	75°f	stock	2 min.
High Contrast Copy /35mm	25	D19	75°f	stock	4 min.
SO 410/35mm	1?0	HC110	68°f	1:19 Dilution F	8 min.
Agfa Geveart 10E75	(?)	HRP	68°f	1:4	1.5 min.

74

Procedure for mapping transforms.

The basic scanning hardware is a prototype unit purchased from Conductron Corp. and consists of:

1) Scanner: a photomultiplier tube completely enclosed except for a pinhole towards the laser and at the height of the system's optic axis. The size of the pinhole can be varied. The photomultiplier can be translated horizontally, orthogonal to the optical axis. The entire assembly can be readily secured to the bed of the optical bench.

2) Photomultiplier power supply: Harrison 6515A DC power supply manufactured by Hewlett-Packard.

3) Ammeter: #414 micro-micro ammeter manufactured by Keithley Instruments.

4) Strip chart recorder: Esterline-Angus dual trace Speed-Serro II.

The phototransparency X-Y-θ input gate is manufactured by Ardel Corp. It consists of two TT-100 translation modules to provide X-Y movement and one RT-175, 360° rotatable module to provide rotation about the optic axis. The stacked modules are mounted with a #275 post, an SID base and a PTT adapter.

The Ardel assembly was modified by the insertion of pins at 90° intervals around the circular opening of the RT-175. These are used for securing the input to the gate. A set screw was also added in order to eliminate rotation about the vertical mounting rod.

General mapping procedure

1. Before the bench is converted to the mapping configuration pictures of the transforms to be mapped and a corresponding calibration transform must be recorded.

2. The highest desired resolvable frequency is determined from the pictures of the transforms.

3. From the time base constants of the recorded and the velocity of the scanner, a maximum "half-transform distance" is determined and the scanner is positioned accordingly.

4. The input gate is placed on the optical bench in its proper position to assure its orthogonality with the optic axis.

5. Opaque tape is used to mask one of two thick optical flats so that when the input is placed on it only the desired rectangular portion of the input will be illuminated.

6. The calibration grid is sandwiched between the two glass flats and mounted on the X-Y-0 input gate. The masked aperture is centered on the optic axis.

7. The viewing microscope is focused on the transform generated by the input in the first transform plane and, using a horizontal knife edge filter, the rotary gate is adjusted so that one arm of the cross generated by the rectangular aperature is parallel to the knife-edge filter.

8. The transform enlarging lens is placed on the bench so that the second transform is approximately focused in the plane of the scanner pinhole.

9. The frequency enlarging lens and the scanner micrometer are adjusted until a maximum reading on the ammeter shows that the transform is properly focused and centered. To aid in focusing, a telemicroscope or other viewing device is sometimes used (in combination with a beamspletter) to view the plane of the scanner pinhole.

10. The scanner is translated one-half transform width and is scanned towards the transform center several times while adjusting the voltage controls of the plotter and those of the ammeter so that the maximum intensity of the DC spot is recorded almost full scale.

11. A full scan of the calibration transform is recorded and compared with the maximum resolvable frequency desired. If unsatisfactory, the position of the scanner is re-adjusted, and then proceed from step #9.

12. After obtaining a satisfactory calibration scan, the first input is inserted, as per steps #6 to #10, and then scanned.

13. The input is rotated through the desired number of degrees, centered and scanned again.

14. The scans are plotted radially in proper orientation using the DC spot as a centering guide.

(Analog unit is being constructed to permit plotting of following functions of intensity: square root, integral, integral of the square root, and square root of the integral)

List of available photographic equipment

*1. Praktina 35mm SLR and adapters for microscope.

2. Speed graphic view camera.

3. Calumet view camera, 4 inch X 5 inch.

4. Hasselblad 500 with standard and wide angle lenses, bellows, light shield, and shutter for photomicrography.

5. Bausch and Lomb/Nikon 135mm telemicroscope.

6. Polaroid photomicrography set-up.

7. Crown Graphic press camera, 4 inch X 5 inch.

8. Bowens Illumitran and accessories.

9. Miranda Automex 35mm SLR camera body.

10. Polaroid 46-L back for view cameras.

11. 120 back for view cameras.

12. Polaroid 4X5 (52, 55, 57) back for view cameras.

**13. Nikon F 35mm SLR and accesscries.

14. Minolta light meter.

15. Zeiss photomicrographic adapter tube.

* adapted to optical diffraction analysis.

** available if needed.

Reduction, Enlargement, and Scaling Relationships
via Measurements on Inputs and Outputs

	Corresponding distances, intervals.	Reduction (enlargement)	Scale	Remarks
Original (Ground distance, distance on peel, micro-slide, etc.)	X_o			Same scale as input for direct processing of thin section or 1:1 photocopy of acetate peel.
Photo, map, line drawing of original. ("Record") (Calibration grid included at this stage)	X_i	$\frac{X_o}{X_i}$	$\frac{X_i}{X_o}$	Often the display "of record", in publication, etc. Work back from calibration grid to original as well as forward to outputs.
Input (reduced transparency)	X_t	$\frac{X_o}{X_t} = \frac{X_o}{X_i} \cdot \frac{X_i}{X_t}$ ------- $\frac{X_i}{X_t}$ (from preceding step)	$\frac{X_t}{X_o}$	This is the "original" in direct processing of thin section ($X_t = X_o$); for contact or 1:1 copy of acetate peel, X_t also $= X_o$.
Transform generated by input	r_1		$K\ (\frac{1}{X_t})$ $K'X_t$	$K = X_t^2\ K'$
Photo, map or profile of transform; TV	r_1'	$e_1 r_1 = \frac{e_1 K_1}{X_t} = e_1 K_1 X_t$ =enlargement of print or TV display of transform	$\frac{r_1'}{r_1} = e_1$	$\frac{r_1'}{X_f'} = \frac{e_1}{e_2} \cdot K_2'$

(Continued)

(Continued)

Reduction, Enlargement, and Scaling Relationships via Measurements on Inputs and Outputs

	Corresponding distances, intervals.	Reduction (enlargement)	Scale	Remarks
Reconstructed (filtered) image	X_f	$\frac{X_o}{X_f} = \frac{X_o}{X_i} \cdot \frac{X_i}{X_t} \cdot \frac{X_t}{X_f}$	$\frac{X_f}{X_o}$ $\frac{X_f}{X_t}$ = enlargement of output with respect to input $= \frac{K_2}{K_1} = \frac{K_1}{K_2'}$ $\frac{X_f}{X_i}$ = relative scale of output with respect to "record"	
Photo (enlarged) of reconstructed image; TV.	X_f'	$\frac{X_f'}{X_f}$ = enlargement of print or TV display of reconstructed image ($=e_2$)	$\frac{X_f'}{X_o}$ = scale of print or TV display or reconstructed image $= e_2 \cdot \frac{X_f}{X_o} = e_2 \frac{K_1'}{K_2'} \cdot \frac{X_t}{X_o}$	See r_1' entry above

X's are corresponding distances in input and output images

r's are corresponding distances in transforms, from center of D.C. spot to first order diffraction.

K is transform scaling factor for spacing in the input K_1', 1/K are transform scaling factors for spatial frequency in the input.

K_1 = K for X_t input to transform plane — Ditto K_1' for K'

K_2 = K for X_f output from transform plane — Ditto K_2' for K'

e = enlargement factors (e_1, transforms, e_2 reconstructed image; enlargement with respect to preceding step.)